

A conservative semi-Lagrangian HWENO method for the Vlasov equation^{*}

Xiaofeng Cai[†] Jianxian Qiu[‡] Jingmei Qiu[§]

February 28, 2022

Abstract: In this paper, we present a high order conservative semi-Lagrangian (SL) Hermite weighted essentially non-oscillatory (HWENO) method for the Vlasov equation based on dimensional splitting [Cheng and Knorr, Journal of Computational Physics, 22(1976)]. The major advantage of HWENO reconstruction, compared with the original WENO reconstruction, is compact. For the split one-dimensional equation, to ensure local mass conservation, we propose a high order SL HWENO scheme in a conservative flux-difference form, following the work in [J.-M. Qiu and A. Christlieb, Journal of Computational Physics, v229(2010)]. Besides performing dimensional splitting for the original 2D problem, we design a proper splitting for equations of derivatives to ensure local mass conservation of the proposed HWENO scheme. The proposed fifth order SL HWENO scheme with the Eulerian CFL condition has been tested to work well in capturing filamentation structures without introducing oscillations. We introduce WENO limiters to control oscillations when the time stepping size is larger than the Eulerian CFL restriction. We perform classical numerical tests on rigid body rotation problem, and demonstrate the performance of our scheme via the Landau damping and two-stream instabilities when solving the Vlasov-Poisson system.

Keywords: Conservative semi-Lagrangian scheme; HWENO reconstruction; Vlasov-Poisson system, Landau damping, Two-stream instability.

1 Introduction

This paper focuses on a high order conservative semi-Lagrangian scheme with high order HWENO reconstruction for the Vlasov-Poisson (VP) simulations based on dimensional splitting. The VP system, arise from

^{*}Research was partially supported by NSFC grants 91230110, 11328104, 11571290, 91530107 and NSF DMS-1217008 and DMS-1522777.

[†]School of Mathematical Sciences, Xiamen University, Xiamen, Fujian, 361005, P.R. China. E-mail: xfc99@126.com.

[‡]School of Mathematical Sciences and Fujian Provincial Key Laboratory of Mathematical Modeling & High-Performance Scientific Computing, Xiamen University, Xiamen, Fujian, 361005, P.R. China. E-mail: jxqiu@xmu.edu.cn.

[§]Department of Mathematics, University of Houston, Houston, 77204. E-mail: jingqiu@math.uh.edu.

collisionless plasma applications, reads as following,

$$\frac{\partial f}{\partial t} + \mathbf{v} \cdot \nabla_{\mathbf{x}} f + \mathbf{E}(t, \mathbf{x}) \cdot \nabla_{\mathbf{v}} f = 0, \quad (1.1)$$

and

$$\mathbf{E}(t, \mathbf{x}) = -\nabla_{\mathbf{x}} \phi(t, \mathbf{x}), \quad -\Delta_{\mathbf{x}} \phi(t, \mathbf{x}) = \rho(t, \mathbf{x}), \quad (1.2)$$

where \mathbf{x} and \mathbf{v} are coordinates in phase space $(\mathbf{x}, \mathbf{v}) \in \mathbb{R}^3 \times \mathbb{R}^3$, \mathbf{E} is the electric field, ϕ is the self-consistent electrostatic potential and $f(t, \mathbf{x}, \mathbf{v})$ is probability distribution function which describes the probability of finding a particle with velocity \mathbf{v} at position \mathbf{x} at time t . The probability distribution function couples to the long range fields via the charge density, $\rho(t, \mathbf{x}) = \int_{\mathbb{R}^3} f(t, \mathbf{x}, \mathbf{v}) d\mathbf{v} - 1$, where we take the limit of uniformly distributed infinitely massive ions in the background. Equations (1.1) and (1.2) have been nondimensionalized so that all physical constants are one.

Popular methods in fusion simulations include Lagrangian, semi-Lagrangian and Eulerian methods. Popular lagrangian methods include the particle-in-cell (PIC) [2, 15, 18], Lagrangian particle methods [3, 12]; Eulerian methods include weighted essentially non-oscillatory (WENO) coupled with Fourier collocation [38], continuous finite element methods [37, 36], Runge-Kutta discontinuous Galerkin methods [1, 11, 17, 8]. Each method has its own advantages and limits. For example, Lagrangian methods are well known for its reasonable low computational cost for high dimensional problems. However, it suffers from statistical noise due to the initial sampling of macro-particles. Eulerian methods offer a good alternative to overcome this lack of precision, but they suffer from 'the curse of dimensionality' and the CFL time step restriction. Compared with the Eulerian approach, the SL methods is relief from the CFL time step restriction, because information is being propagated along characteristics.

Among SL schemes, the scheme based on dimensional splitting, introduced by Cheng and Knorr originally [7], is very popular SL scheme with high order cubic spline interpolation was proposed in [31]. A positivity preserving and flux conservative finite volume SL scheme with ENO reconstruction for the VP system is proposed in [14] and the scheme for the guiding center Vlasov model is proposed in [10]. A conservative finite different semi-Lagrangian scheme with WENO reconstruction is proposed in [25]; later the algorithm is generalized to variable coefficient case [26, 27] and maximum principle preserving limiter [33]. In the finite element discontinuous Galerkin framework, there are SL discontinuous Galerkin schemes with positivity preserving limiters [28, 29] and hybrid SL finite element-finite difference methods in [16]. High order propagation methods based on Hermite

interpolation are proposed in [22, 13, 5, 4, 35]. HWENO scheme was introduced in [23] and further developed in [39, 21] for hyperbolic conservation laws. Besides the original equation, one also evolves equations of derivatives in the WENO fashion. Hence their reconstruction stencils are more compact than the original WENO scheme [19], given the same order of approximation. A similar technique, called the CIP (Constrained Interpolation Profile/Cubic Interpolated Propagation) scheme [34], has also been proposed for the VP system [22]. In [5], besides the function values themselves, the gradients of the function are evolved in a semi-Lagrangian fashion. In [35], a semi-Lagrangian HWENO is proposed without evolving the gradients. The proposed method in this paper successfully couples the semi-Lagrangian framework with HWENO method. Compared with those earlier work, our method achieves local mass conservation, has relatively compact stencil and is able to capture under-resolve solution structures without numerical artifacts.

In this paper, we design a conservative SL HWENO scheme based on dimensional splitting. Its stencil is more compact than the regular WENO scheme. We follow the idea in [25] to express the SL update in a flux difference conservative form. There are several new ingredients we developed in this paper in order to ensure the effectiveness and robustness of the proposed scheme: firstly, we design a SL HWENO scheme in a flux difference form for 1D problem; secondly, we apply a special splitting similar to the splitting in the CIP method [22] for mass conservation for high dimensional problems; thirdly, we introduce WENO limiters for controlling oscillations.

The paper is organized as follows. In Section 2, we introduce a conservative form of high order SL HWENO method for 1D transport problems. In Section 3, we introduce a conservative SL HWENO for VP system by a special form of splitting, and introduce WENO limiters. In Section 4, we present our numerical results for basic test problems, such as linear advection and rigid body rotation, and for the VP simulations. Concluding remarks are given in Section 5.

2 Conservative SL HWENO method for 1D transport problem

In this section, we introduce the SL Hermite interpolation in a flux-difference form for 1D transport problems. Then we incorporate the HWENO mechanism into the flux function reconstruction procedure to realize a non-oscillatory capturing of shocks.

2.1 The SL Hermite interpolation in a flux-difference form for 1D transport problem

In this section, we consider a 1D transport problem

$$f_t + vf_x = 0, \quad f(x, t = 0) = f_0(x), \quad \text{on } [a, b], \quad (2.1)$$

where v is a constant. For the Hermite method, we also consider the evolution equation for the solution's derivative $g \doteq f_x$. For the linear transport problem (2.1), g satisfies the same linear transport equation

$$g_t + vg_x = 0.$$

We discretize the domain $[a, b]$ as

$$a = x_{\frac{1}{2}} < x_{\frac{3}{2}} < \cdots < x_{N+\frac{1}{2}} = b,$$

with the uniform grid points $x_i = a + (i - \frac{1}{2})\Delta x$ and the cell size $\Delta x = x_{i+\frac{1}{2}} - x_{i-\frac{1}{2}}$. We let $I_i = [x_{i-\frac{1}{2}}, x_{i+\frac{1}{2}}]$ and $I_{i+\frac{1}{2}} = [x_i, x_{i+1}]$. In the HWENO approach, the numerical solutions associated with each grid point are point values f_i^n and derivatives g_i^n . Here the subscript i means the solution at the grid point x_i and the superscript n means the solution at time level t^n . To design a SL HWENO scheme, we update $\{f_i^{n+1}, g_i^{n+1}\}_{i=1}^N$ from the corresponding solutions at time t^n .

For the linear problem (2.1) with constant characteristic speed, the solutions f_i^{n+1} and g_i^{n+1} can be obtain by shifting the information at t^n in the SL framework. We define the amount of shift $\frac{v\Delta t}{\Delta x}$ as $xshift$. There are three cases of $xshift$: shift to the right by some amount less than half a cell ($xshift \in [0, \frac{1}{2}]$), shift to the left by some amount less than half a cell ($xshift \in [-\frac{1}{2}, 0]$) and shift a distance greater than half a cell ($|xshift| > \frac{1}{2}$).

To illustrate the idea, we only consider Hermite interpolations for $xshift \in [0, \frac{1}{2}]$, while the one for $xshift \in [-\frac{1}{2}, 0]$ is mirror symmetric with respect to x_i of the previous interpolations. In the case when $|xshift| > \frac{1}{2}$, whole grid shifting is carried out and followed by a final update based on the procedure for $xshift \in [-\frac{1}{2}, \frac{1}{2}]$. In the following, we present the Hermite interpolation with cubic polynomials. Higher order schemes will be discussed later.

1. The underlying function at t^n can be approximated by a Hermite-type reconstruction, based on the stencil

$$\{f_{i-1}^n, f_i^n, g_{i-1}^n, g_i^n\},$$

$$\begin{aligned} \tilde{f}_{i-\frac{1}{2}}^n(\xi) &= f_i^n - g_i^n \Delta x \xi + (2g_i^n \Delta x - 3f_i^n + 3f_{i-1}^n + g_{i-1}^n \Delta x) \xi^2 \\ &\quad + (2f_i^n - g_i^n \Delta x - 2f_{i-1}^n - g_{i-1}^n \Delta x) \xi^3, \end{aligned}$$

where $\xi(x) = \frac{x-x_i}{x_{i-1}-x_i} \in [0, 1], x \in I_{i-\frac{1}{2}}$.

2. f_i^{n+1} and g_i^{n+1} can be obtained by tracing the characteristic back to time $t = t^n$ and evaluating the interpolant $\tilde{f}_{i-\frac{1}{2}}^n(\xi)$ at the foot of characteristics $x^* = x_i - v\Delta t$,

$$\begin{aligned} f_i^{n+1} &= f_i^n - \xi_0((3f_i^n \xi_0 - 2f_i^n \xi_0^2) - (3f_{i-1}^n \xi_0 - 2f_{i-1}^n \xi_0^2)) \\ &\quad - g_i^n \Delta x \xi_0 + (2g_i^n \Delta x + g_{i-1}^n \Delta x) \xi_0^2 + (-g_i^n \Delta x - g_{i-1}^n \Delta x) \xi_0^3 \end{aligned} \quad (2.2)$$

$$\begin{aligned} g_i^{n+1} &= g_i^n + \left(-4g_i^n + \frac{6f_i^n - 6f_{i-1}^n}{\Delta x} - 2g_{i-1}^n \right) \xi_0 \\ &\quad + \left(-\frac{6f_i^n - f_{i-1}^n}{\Delta x} + 3g_i^n + 3g_{i-1}^n \right) \xi_0^2, \end{aligned} \quad (2.3)$$

where $\xi_0 = \frac{x^* - x_i}{x_{i-1} - x_i}$.

For the above linear scheme (2.2) and (2.3), we have the following mass conservation result.

PROPOSITION 1. *If $\sum_{i=1}^N g_i^n \equiv 0$ and with periodic boundary condition, then the scheme (2.2) and (2.3) conserve the total mass, i.e., $\sum_{i=1}^N f_i^{n+1} \equiv \sum_{i=1}^N f_i^n$ and $\sum_{i=1}^N g_i^{n+1} \equiv 0$.*

Proof:

$$\begin{aligned} \sum_{i=1}^N f_i^{n+1} &= \sum_{i=1}^N [f_i^n - \xi_0((3f_i^n \xi_0 - 2f_i^n \xi_0^2) - (3f_{i-1}^n \xi_0 - 2f_{i-1}^n \xi_0^2)) \\ &\quad - g_i^n \Delta x \xi_0 + (2g_i^n \Delta x + g_{i-1}^n \Delta x) \xi_0^2 + (-g_i^n \Delta x - g_{i-1}^n \Delta x) \xi_0^3] \\ &= \sum_{i=1}^N f_i^n - \xi_0((3f_N^n \xi_0 - 2f_N^n \xi_0^2) - (3f_0^n \xi_0 - 2f_0^n \xi_0^2)) \\ &\quad + \sum_{i=1}^N g_{i-1}^n \Delta x \xi_0^2 - \sum_{i=1}^N g_{i-1}^n \Delta x \xi_0^3 \\ &= \sum_{i=1}^N f_i^n \text{ (periodic boundary condition),} \end{aligned}$$

$$\begin{aligned} \sum_{i=1}^N g_i^{n+1} &= \sum_{i=1}^N \left[g_i^n + \left(-4g_i^n + \frac{6f_i^n - 6f_{i-1}^n}{\Delta x} - 2g_{i-1}^n \right) \xi_0 \right. \\ &\quad \left. + \left(-\frac{6f_i^n - f_{i-1}^n}{\Delta x} + 3g_i^n + 3g_{i-1}^n \right) \xi_0^2 \right] \\ &= \sum_{i=1}^N g_i^n + \frac{6f_N^n - 6f_0^n}{\Delta x} \xi_0 - \frac{6f_N^n - f_0^n}{\Delta x} \xi_0^2 + 2 \sum_{i=1}^N g_{i-1}^n \Delta x \xi_0^2 - 3 \sum_{i=1}^N g_{i-1}^n \Delta x \xi_0^3 \\ &= \sum_{i=1}^N g_i^n \text{ (periodic boundary condition).} \end{aligned}$$

Hence the proposition is proved. ■

In order to guarantee $\sum_{i=1}^N g_i^0 \equiv 0$ in the assumption of the proposition, we introduce a sliding average function $h(x)$ in [30] which satisfies

$$f(x) = \frac{1}{\Delta x} \int_{x-\frac{\Delta x}{2}}^{x+\frac{\Delta x}{2}} h(\xi) d\xi,$$

then

$$g(x) = f(x)_x = \frac{1}{\Delta x} \left(h\left(x + \frac{\Delta x}{2}\right) - h\left(x - \frac{\Delta x}{2}\right) \right).$$

Thus $\sum_{i=1}^N g_i^0 = \sum_{i=1}^N (h_{i+\frac{1}{2}}^0 - h_{i-\frac{1}{2}}^0) \equiv 0$ where $h_{i\pm\frac{1}{2}}^0 \approx h(x \pm \frac{\Delta x}{2})$ can be obtained by reconstruction from $\{f_j^0\}_j$.

In the following, we will adopt a matrix notation for presentation of the Hermite interpolation. The matrix A will denote the interpolation matrix. We use $A(i, j)$ to denote the element at the i^{th} row and j^{th} column, $A(i, :)$ to denote the i^{th} row of A , and $A(:, j)$ to denote the j^{th} column of A .

We rewrite the scheme (2.2) and (2.3) into a flux difference form, in order to ensure local mass conservation, especially when the nonlinear HWENO mechanism is applied. In order to do so, we propose to update $\{f_i^n, h_{i+\frac{1}{2}}^n\}_i$ instead of $\{f_i^n, g_i^n\}_i$, observing that g_i^n can be recovered from $\{h_{i+\frac{1}{2}}^n\}_i$ by $g_i^n = (h_{i+\frac{1}{2}}^n - h_{i-\frac{1}{2}}^n) / \Delta x$. Specifically, (2.2) can be rewritten in the following flux difference form using the new $\{h_{i+\frac{1}{2}}^n\}_i$,

$$\begin{aligned} f_i^{n+1} &= f_i^n - \xi_0((3f_i^n \xi_0 - 2f_i^n \xi_0^2) - (3f_{i-1}^n \xi_0 - 2f_{i-1}^n \xi_0^2)) \\ &\quad - g_i^n \Delta x \xi_0 + (2g_i^n \Delta x + g_{i-1}^n \Delta x) \xi_0^2 + (-g_i^n \Delta x - g_{i-1}^n \Delta x) \xi_0^3 \\ &= f_i^n - \xi_0(f_i^n(3\xi_0 - 2\xi_0^2) - f_{i-1}^n(3\xi_0 - 2\xi_0^2)) + g_i^n \Delta x(-\xi_0 + 2\xi_0^2 - \xi_0^3) + g_{i-1}^n \Delta x(\xi_0^2 - \xi_0^3) \\ &= f_i^n - \xi_0(f_i^n(3\xi_0 - 2\xi_0^2) - f_{i-1}^n(3\xi_0 - 2\xi_0^2)) \\ &\quad - \left(h_{i+\frac{1}{2}}^n - h_{i-\frac{1}{2}}^n\right) \xi_0(1 - 2\xi_0 + \xi_0^2) - \left(h_{i-\frac{1}{2}}^n - h_{i-\frac{3}{2}}^n\right) \xi_0(-\xi_0 + \xi_0^2) \\ &= f_i^n - \xi_0 \left\{ \left[f_i^n(3\xi_0 - \xi_0^2) + h_{i+\frac{1}{2}}^n(1 - 2\xi_0 + \xi_0^2) + h_{i-\frac{1}{2}}^n(-\xi_0 - \xi_0^2) \right] \right. \\ &\quad \left. - \left[f_{i-1}^n(3\xi_0 - \xi_0^2) + h_{i-\frac{1}{2}}^n(1 - 2\xi_0 + \xi_0^2) + h_{i-\frac{3}{2}}^n(-\xi_0 - \xi_0^2) \right] \right\} \\ &= f_i - \xi_0(\widehat{f}_{i+\frac{1}{2}}^n(\xi_0) - \widehat{f}_{i-\frac{1}{2}}^n(\xi_0)). \end{aligned}$$

where

$$\widehat{f}_{i-\frac{1}{2}}^n(\xi_0) = (f_{i-1}^n, h_{i-\frac{1}{2}}^n, h_{i-\frac{3}{2}}^n) \cdot C_3^L \cdot (1, \xi_0, \xi_0^2)'$$

with

$$C_3^L = \begin{pmatrix} 0 & 3 & -2 \\ 1 & -2 & 1 \\ 0 & -1 & 1 \end{pmatrix}.$$

We update g_i^{n+1} by

$$g_i^{n+1} = \frac{h_{i+\frac{1}{2}}^{n+1} - h_{i-\frac{1}{2}}^{n+1}}{\Delta x} \quad (2.4)$$

where

$$h_{i-\frac{1}{2}}^{n+1} = (f_{i-1}^n, h_{i-\frac{1}{2}}^n, h_{i-\frac{3}{2}}^n) \cdot D_3^L \cdot (1, \xi_0, \xi_0^2)' \quad (2.5)$$

with

$$D_3^L = \begin{pmatrix} 0 & 6 & -6 \\ 1 & -4 & 3 \\ 0 & -2 & 3 \end{pmatrix}.$$

REMARK 1. *The flux-difference form for the SL finite difference scheme was originally proposed in [25].*

There are two main advantages to work with the flux difference form:

1. *The flux difference form can ensure local mass conservation.*
2. *We can design a nonlinear HWENO mechanism for the flux reconstructions, see discussions in the next subsection.*

In order to work with the flux difference form, it is crucial to work with the $\{h_{i+\frac{1}{2}}^n\}_i$ instead of the original derivative function $g = f_x$.

REMARK 2. *We observe that $D_3^L(:, k) = kC_3^L(:, k)$, $k = 1, 2, 3$.*

REMARK 3. *The case presented here is for the third order scheme. Similar procedure can be used to obtained higher order scheme, e.g. the fifth order case with HWENO is presented in the next subsection.*

2.2 HWENO reconstruction for flux functions

In general, high order fixed stencil reconstruction of numerical fluxes performs well when the solution is smooth. However, around discontinuities, oscillations will be introduced. In this subsection, a nonlinear SL HWENO procedure is introduced for reconstructing the flux $\widehat{f}_{i-\frac{1}{2}}^n(\xi)$. By adaptively assigning nonlinear weights to neighboring candidate stencils, the nonlinear HWENO reconstruction preserves high order accuracy of the linear scheme around smooth regions of the solution, while producing a sharp and essentially non-oscillatory capture of discontinuities.

We adopt the idea of the HWENO reconstruction [23, 21] into the proposed conservative SL framework. We present a fifth order HWENO reconstruction as an example. Similar procedure can be generalized to higher order case.

Our discussion will be focused on the case of $xshift \in [-\frac{1}{2}, \frac{1}{2}]$. As before, the case of $|xshift| > \frac{1}{2}$ will be handled with a whole grid shift followed by the case of $xshift \in [-\frac{1}{2}, \frac{1}{2}]$ to account for the fractional remainder.

When $xshift \in [0, \frac{1}{2}]$, the fifth order conservative SL method the $\{f_{i-2}^n, f_{i-1}^n, f_i^n, f_{i+1}^n, g_{i-2}^n, g_{i+1}^n\}$ is the following,

$$\begin{aligned} f_i^{n+1} = & f_i^n + \left(-\frac{8}{27}f_{i-2}^n + f_{i-1}^n - \frac{19}{27}f_{i+1}^n + \frac{2}{9}g_{i+1}^n\Delta x - \frac{1}{9}g_{i-2}^n\Delta x \right) \xi_0 \\ & + \left(-\frac{1}{18}g_{i-2}^n\Delta x - \frac{2}{9}g_{i+1}^n\Delta x - \frac{7}{4}f_i^n - \frac{19}{108}f_{i-2}^n + f_{i-1}^n + \frac{25}{27}f_{i+1}^n \right) \xi_0^2 \\ & + \left(\frac{1}{6}g_{i-2}^n\Delta x - \frac{1}{6}g_{i+1}^n\Delta x + \frac{1}{4}f_i^n + \frac{5}{12}f_{i-2}^n - \frac{3}{4}f_{i-1}^n + \frac{1}{12}f_{i+1}^n \right) \xi_0^3 \\ & + \left(\frac{1}{18}g_{i-2}^n\Delta x + \frac{2}{9}g_{i+1}^n\Delta x + \frac{3}{4}f_i^n + \frac{19}{108}f_{i-2}^n - \frac{1}{2}f_{i-1}^n - \frac{23}{54}f_{i+1}^n \right) \xi_0^4 \\ & + \left(-\frac{1}{18}g_{i-2}^n\Delta x - \frac{1}{18}g_{i+1}^n\Delta x - \frac{1}{4}f_i^n - \frac{13}{108}f_{i-2}^n + \frac{1}{4}f_{i-1}^n + \frac{13}{108}f_{i+1}^n \right) \xi_0^5, \end{aligned}$$

Using the flux difference form for g function, $g_i^n = \frac{h_{i+\frac{1}{2}}^n - h_{i-\frac{1}{2}}^n}{\Delta x}$ in t^n , then

$$f_i^{n+1} = f_i^n - \xi_0((f_{i-2}^n, f_{i-1}^n, f_i^n, f_{i+1}^n, h_{i-\frac{5}{2}}^n, h_{i-\frac{3}{2}}^n, h_{i+\frac{1}{2}}^n, h_{i+\frac{3}{2}}^n) \cdot B_5^L \cdot (1, \xi_0, \xi_0^2, \xi_0^3, \xi_0^4)')$$

where

$$B_5^L = \begin{pmatrix} \frac{8}{27} & \frac{19}{108} & -\frac{5}{12} & -\frac{19}{108} & \frac{13}{108} \\ -1 & -1 & \frac{3}{4} & \frac{2}{3} & -\frac{1}{4} \\ 0 & \frac{7}{4} & -\frac{1}{4} & -\frac{4}{23} & \frac{1}{4} \\ \frac{19}{27} & -\frac{25}{27} & -\frac{1}{12} & \frac{23}{54} & -\frac{13}{108} \\ -\frac{1}{9} & -\frac{1}{18} & \frac{1}{6} & \frac{1}{18} & -\frac{1}{18} \\ \frac{1}{9} & \frac{1}{18} & -\frac{1}{6} & -\frac{1}{18} & \frac{1}{18} \\ -\frac{2}{9} & \frac{2}{9} & \frac{1}{6} & -\frac{2}{9} & -\frac{1}{18} \end{pmatrix}.$$

Then f_i^{n+1} can be written in the flux difference form,

$$f_i^{n+1} = f_i^n - \xi_0((f_{i-1}^n, f_i^n, f_{i+1}^n, h_{i-\frac{3}{2}}^n, h_{i+\frac{3}{2}}^n) \cdot C_5^L - (f_{i-2}^n, f_{i-1}^n, f_i^n, h_{i-\frac{5}{2}}^n, h_{i+\frac{1}{2}}^n) \cdot C_5^L) \cdot (1, \xi_0, \xi_0^2, \xi_0^3, \xi_0^4)' \quad (2.6)$$

where

$$C_5^L = \begin{pmatrix} -\frac{8}{27} & -\frac{19}{108} & \frac{5}{12} & \frac{19}{108} & -\frac{13}{108} \\ \frac{19}{27} & \frac{25}{27} & -\frac{1}{12} & -\frac{23}{54} & \frac{13}{108} \\ \frac{1}{9} & \frac{1}{18} & -\frac{1}{6} & -\frac{1}{18} & \frac{1}{18} \\ -\frac{2}{9} & \frac{2}{9} & \frac{1}{6} & -\frac{2}{9} & -\frac{1}{18} \end{pmatrix}$$

And we have the flux difference form the derivative g_i^{n+1} in t^{n+1} ,

$$g_i^{n+1} = \frac{h_{i+\frac{1}{2}}^{n+1} - h_{i-\frac{1}{2}}^{n+1}}{\Delta x}$$

where

$$h_{i-\frac{1}{2}}^{n+1} = (f_{i-2}^n, f_{i-1}^n, f_i^n, h_{i-\frac{5}{2}}^n, h_{i+\frac{1}{2}}^n) \cdot D_5^L \cdot (1, \xi_0, \xi_0^2, \xi_0^3, \xi_0^4)' \quad (2.7)$$

where D_5^L satisfies $D_5^L(:, k) = kC_5^L(:, k)$, $k = 1, \dots, 5$.

When $xshift \in [-\frac{1}{2}, 0]$, we update $\{f_i^{n+1}, h_{i+\frac{1}{2}}^{n+1}\}_i$ by the following formulas,

$$f_i^{n+1} = f_i^n + \xi_0(\widehat{f}_{i+\frac{1}{2}}^n(\xi_0) - \widehat{f}_{i-\frac{1}{2}}^n(\xi_0)), \quad (2.8)$$

where the flux function

$$\widehat{f}_{i-\frac{1}{2}}^n(\xi) = (f_{i-1}^n, f_i^n, f_{i+1}^n, h_{i-\frac{3}{2}}^n, h_{i+\frac{3}{2}}^n) \cdot C_5^R \cdot (1, \xi_0, \xi_0^2, \xi_0^3, \xi_0^4)', \quad (2.9)$$

where

$$C_5^R = \begin{pmatrix} \frac{19}{27} & -\frac{25}{27} & -\frac{1}{12} & \frac{23}{54} & -\frac{13}{108} \\ \frac{19}{27} & \frac{89}{108} & -\frac{1}{3} & -\frac{35}{108} & \frac{7}{54} \\ -\frac{8}{27} & -\frac{19}{108} & \frac{5}{12} & \frac{19}{108} & -\frac{13}{108} \\ -\frac{2}{9} & \frac{2}{9} & \frac{1}{6} & -\frac{2}{9} & \frac{1}{18} \\ \frac{1}{9} & \frac{1}{18} & -\frac{1}{6} & -\frac{1}{18} & \frac{1}{18} \end{pmatrix}. \quad (2.10)$$

And

$$h_{i-\frac{1}{2}}^{n+1} = (f_{i-1}^n, f_i^n, f_{i+1}^n, h_{i-\frac{3}{2}}^n, h_{i+\frac{3}{2}}^n) \cdot D_5^R \cdot (1, \xi_0, \xi_0^2, \xi_0^3, \xi_0^4)' \quad (2.11)$$

where D_5^R satisfies $D_5^R(:, k) = kC_5^R(:, k)$, $k = 1, \dots, 5$.

In the following, we illustrate the corresponding HWENO reconstruction of flux functions. We only discuss the HWENO reconstruction for the flux $\widehat{f}_{i-\frac{1}{2}}^n$ and $h_{i-\frac{1}{2}}^{n+1}$ when $xshift \in [0, \frac{1}{2}]$. When $xshift \in [-\frac{1}{2}, 0]$, the flux $\widehat{f}_{i-\frac{1}{2}}^n$ and $h_{i-\frac{1}{2}}^{n+1}$ could be reconstructed symmetrically with respect to x_i . From equations (2.6) and (2.7), the stencil $\{f_{i-2}^n, f_{i-1}^n, f_i^n, h_{i-\frac{5}{2}}^n, h_{i+\frac{1}{2}}^n\}$ is used to construct the flux $\widehat{f}_{i-\frac{1}{2}}^n(\xi)$ and $h_{i-\frac{1}{2}}^{n+1}$. It is composed of the information from three potential stencils

$$S_1 = \{h_{i-\frac{5}{2}}^n, f_{i-2}^n, f_{i-1}^n\}, \quad S_2 = \{f_{i-2}^n, f_{i-1}^n, f_i^n\}, \quad S_3 = \{f_{i-1}^n, f_i^n, h_{i+\frac{1}{2}}^n\}. \quad (2.12)$$

Intuitively, in regions where the function is smooth, we want to use information from S_1, S_2 and S_3 in an optimal way, to obtain a fifth order approximation. On the other hand, around a big jump, we only want to use the information from the relatively smooth stencil. Following [25], we only use the HWENO mechanism in adaptively reconstructing the coefficients in front of the constant 1 in the equation for $\widehat{f}_{i-\frac{1}{2}}^n$ and $h_{i-\frac{1}{2}}^{n+1}$, while leaving coefficients for $\xi_0, \xi_0^2, \xi_0^3, \xi_0^4$ unchanged. We can observe that the first column of matrix C_5^L is the same as that of D_5^L . Thus we only consider the HWENO procedure for constructing $\widehat{f}_{i-\frac{1}{2}}^n$,

1. Compute the linear weights, γ_1, γ_2 and γ_3 , such that

$$\begin{aligned} & (f_{i-2}^n, f_{i-1}^n, f_i^n, h_{i-\frac{5}{2}}^n, h_{i+\frac{1}{2}}^n) \cdot C_5^L(:, 1) \\ &= \gamma_1(f_{i-2}^n, f_{i-1}^n, h_{i-\frac{5}{2}}^n) \cdot (-2, 2, 1)' + \gamma_2(f_{i-2}^n, f_{i-1}^n, f_i^n) \cdot (-\frac{1}{6}, \frac{5}{6}, \frac{1}{3})' \\ &+ \gamma_3(f_{i-1}^n, f_i^n, h_{i+\frac{1}{2}}^n) \cdot (\frac{1}{4}, \frac{5}{4}, -\frac{1}{2})', \end{aligned}$$

where $(f_{i-2}^n, f_{i-1}^n, h_{i-\frac{5}{2}}^n) \cdot (-2, 2, 1)'$, $(f_{i-2}^n, f_{i-1}^n, f_i^n) \cdot (-\frac{1}{6}, \frac{5}{6}, \frac{1}{3})'$ and $(f_{i-1}^n, f_i^n, h_{i+\frac{1}{2}}^n) \cdot (\frac{1}{4}, \frac{5}{4}, -\frac{1}{2})'$ are third order reconstructions of fluxes from three stencils S_1, S_2 and S_3 respectively. From equation (2.6), $\gamma_1 = \frac{1}{9}$, $\gamma_2 = \frac{4}{9}$ and $\gamma_3 = \frac{4}{9}$.

2. We compute the smoothness indicator, denoted by β_j , for each stencil S_j , which measures how smooth the function $p_j(x)$ is in the target cell I_i . The smaller this smoothness indicator β_j , the smoother the function $p_j(x)$ is in the target cell. We use the same recipe for the smoothness indicator as in [19],

$$\beta_j = \sum_{l=1}^2 \int_{I_i} \Delta x^{2l-1} \left(\frac{\partial}{\partial x^l} p_j(x) \right)^2 dx.$$

In the actual numerical implementation the smoothness indicators β_j are written out explicitly as quadratic forms of the points $\{f_i^n, h_{i+\frac{1}{2}}^n\}_i$ in the stencil,

$$\begin{aligned} \beta_1 &= \frac{13}{3} \left(-\frac{9}{4} f_{i-2}^n + \frac{3}{2} h_{i-\frac{5}{2}}^n + \frac{3}{4} f_{i-1}^n \right)^2 + \left(\frac{31}{4} f_{i-2}^n - \frac{9}{2} h_{i-\frac{5}{2}}^n - \frac{13}{4} f_{i-1}^n \right)^2, \\ \beta_2 &= \frac{13}{12} (-f_{i-2}^n + 2f_{i-1}^n - f_i^n)^2 + \left(-\frac{3}{2} f_i^n + 2f_{i-1}^n - \frac{1}{2} f_{i-2}^n \right)^2, \\ \beta_3 &= \frac{13}{3} \left(-\frac{9}{4} f_i^n + \frac{3}{4} f_{i-1}^n + \frac{3}{2} h_{i+\frac{1}{2}}^n \right)^2 + \left(\frac{5}{4} f_i^n + \frac{1}{4} f_{i-1}^n - \frac{3}{2} h_{i+\frac{1}{2}}^n \right)^2. \end{aligned}$$

3. We compute the nonlinear weights based on the smoothness indicators.

$$\omega_j = \frac{\bar{\omega}_j}{\sum_{k=1}^3 \bar{\omega}_k}, \quad j = 1, 2, 3, \quad \bar{\omega}_k = \frac{\gamma_k}{\epsilon + \beta_k}$$

where ϵ is a small number to prevent the denominator to becoming zero. In our numerical tests we take ϵ to be 10^{-6} .

4. Compute numerical fluxes constructed in HWENO fashion. Define the matrix \tilde{C}_5^L and \tilde{D}_5^L as,

$$\tilde{D}_5^L(:, 1) = \tilde{C}_5^L(:, 1) = \omega_1 \cdot (-2, 2, 0, 1, 0) + \omega_2 \cdot \left(-\frac{1}{6}, \frac{5}{6}, \frac{1}{3}, 0, 0\right) + \omega_3 \cdot \left(0, \frac{1}{4}, \frac{5}{4}, 0, -\frac{1}{2}\right)$$

$$\tilde{C}_5^L(:, k) = C_5^L(:, k), \quad \tilde{D}_5^L(:, 2) = k C_5^L(:, k), \quad k = 2, \dots, 5.$$

The updated numerical flux is computed using \tilde{C}_5^L and \tilde{D}_5^L , i.e.,

$$\hat{f}_{i-\frac{1}{2}}^n(\xi_0) = (f_{i-2}^n, f_{i-1}^n, f_i^n, h_{i-\frac{5}{2}}^n, h_{i+\frac{1}{2}}^n) \cdot \tilde{C}_5^L \cdot (1, \xi_0, \xi_0^2, \xi_0^3, \xi_0^4)', \quad (2.13)$$

$$h_{i-\frac{1}{2}}^{n+1} = (f_{i-2}^n, f_{i-1}^n, f_i^n, h_{i-\frac{5}{2}}^n, h_{i+\frac{1}{2}}^n) \cdot \tilde{D}_5^L \cdot (1, \xi_0, \xi_0^2, \xi_0^3, \xi_0^4)'. \quad (2.14)$$

3 Strang splitting SL HWENO scheme for the VP system

In this section, we extend the SL HWENO scheme in the previous section for solving the 1D VP system.

Denoting by $f(t, x, v) \geq 0$ the distribution function of electrons in phase space and by $E(t, x)$ the self-consistent electric field, the dimensionless VP systems reads as

$$\frac{\partial f}{\partial t} + v \frac{\partial f}{\partial x} + E(t, x) \frac{\partial f}{\partial v} = 0, \quad (3.1)$$

$$\frac{dE}{dx}(t, x) = \rho(t, x) = \int_{-\infty}^{+\infty} f(t, x, v) dv - 1, \quad (3.2)$$

on the domain $[a, b] \times [-L, L]$ with periodic boundary condition for the spatial domain and zero boundary condition for the velocity domain.

For the Hermite method, we advect not only the distribution function f but also the its gradients of f in x and in v directions. We have the following equations for f_x and f_v ,

$$\begin{cases} \frac{\partial f_x}{\partial t} + v \frac{\partial f_x}{\partial x} + \frac{\partial(E(t, x)f_v)}{\partial x} = 0, \\ \frac{\partial f_v}{\partial t} + \frac{\partial(vf_x)}{\partial v} + E(t, x) \frac{\partial f_v}{\partial v} = 0. \end{cases} \quad (3.3)$$

In this section, the SL HWENO scheme solve this system based on the Strang splitting method [7]. The set of governing equations (3.1) and (3.3) of the Strang splitting method is replaced by

$$(SL_x) \begin{cases} \frac{\partial f}{\partial t} + v \frac{\partial f}{\partial x} = 0 & (SL_x^0) \\ \frac{\partial f_x}{\partial t} + v \frac{\partial f_x}{\partial x} = 0 & (SL_x^1) \\ \frac{\partial f_v}{\partial t} + \frac{\partial(vf_x)}{\partial v} = 0 & (FD_x) \end{cases} \quad (3.4)$$

and

$$(SL_v) \begin{cases} \frac{\partial f}{\partial t} + E(t, x) \frac{\partial f}{\partial v} = 0 & (SL_v^0) \\ \frac{\partial f_v}{\partial t} + E(t, x) \frac{\partial f_v}{\partial v} = 0 & (SL_v^1) \\ \frac{\partial f_x}{\partial t} + \frac{\partial(E(t, x)f_v)}{\partial x} = 0 & (FD_v) \end{cases} \quad (3.5)$$

First we solve the system (SL_x) on half a time step, then we solve the system (SL_v) on a time step, and finally solve again the system (SL_x) on half a time step. We will focus our discussion on solving (SL_x) in the following section.

We discretize the computational domain $[a, b] \times [-L, L]$ as $a = x_{\frac{1}{2}} < x_{\frac{3}{2}} < \dots < x_{N_x + \frac{1}{2}} = b$, $-L = v_{\frac{1}{2}} < v_{\frac{3}{2}} < \dots < v_{N_v + \frac{1}{2}} = L$, with uniformly distributed grid points, i.e. $x_i = a + (i - \frac{1}{2})\Delta x$, $v_j = -L + (j - \frac{1}{2})\Delta v$ where grid spacing $\Delta x = x_{i+\frac{1}{2}} - x_{i-\frac{1}{2}}$, $\Delta v = v_{j+\frac{1}{2}} - v_{j-\frac{1}{2}}$. We let $I_i = [x_{i-\frac{1}{2}}, x_{i+\frac{1}{2}}]$, $\forall i = 1, \dots, N_x$, $J_j = [v_{j-\frac{1}{2}}, v_{j+\frac{1}{2}}]$, $\forall j = 1, \dots, N_v$ and $T_{ij} = [x_{i-\frac{1}{2}}, x_{i+\frac{1}{2}}] \times [v_{j-\frac{1}{2}}, v_{j+\frac{1}{2}}]$.

We let f_{ij}^n , $(f_x)_{ij}^n$ and $(f_v)_{ij}^n$ denote the numerical approximation to the solution $f(x_i, v_j)$, $f_x(x_i, v_j)$, $f_v(x_i, v_j)$ at the time t^n respectively. Similar to the 1D problem, we introduce $\{\Phi_{i-\frac{1}{2}, j}^n\}_{ij}$ and $\{\Psi_{i, j-\frac{1}{2}}^n\}_{ij}$ such that

$$(f_x)_{ij}^n = \frac{\Phi_{i+\frac{1}{2}, j}^n - \Phi_{i-\frac{1}{2}, j}^n}{\Delta x}, \quad (f_v)_{ij}^n = \frac{\Psi_{i, j+\frac{1}{2}}^n - \Psi_{i, j-\frac{1}{2}}^n}{\Delta v}$$

In this section, we design a scheme for solving (SL_x) from t^n to t^{n+1} . The scheme for (SL_v) would be similar to that for (SL_x) .

Initialization: We use the high order WENO scheme in [19] to reconstruct $\{\Phi_{i+\frac{1}{2},j}^0\}$ and $\{\Psi_{i,j+\frac{1}{2}}^0\}$ in x -direction and v -direction respectively.

Update: We update $\{f_{ij}^n, \Phi_{i+\frac{1}{2},j}^n\}_{ij}$ by the SL HWENO scheme in Section 2. We update $\Psi_{i,j+\frac{1}{2}}^n$ by the third equation in (3.4) via treating the derivative term as a source term. In particular, we apply the following a central difference scheme coupled with a trapezoid rule for (FD_x) ,

$$(f_v)_{ij}^{n+1} = (f_v)_{ij}^n - \frac{\Delta t}{2} \left(\frac{v_{i,j-2}(f_x)_{i,j-2}^n - 8v_{i,j-1}(f_x)_{i,j-1}^n + 8v_{i,j+1}(f_x)_{i,j+1}^n - v_{i,j+2}(f_x)_{i,j+2}^n}{24\Delta y} \right. \\ \left. \frac{v_{i,j-2}(f_x)_{i,j-2}^{n+1} - 8v_{i,j-1}(f_x)_{i,j-1}^{n+1} + 8v_{i,j+1}(f_x)_{i,j+1}^{n+1} - v_{i,j+2}(f_x)_{i,j+2}^{n+1}}{24\Delta y} \right) \quad (3.6)$$

where

$$(f_x)_{ij}^* = \frac{\Phi_{i+\frac{1}{2},j}^* - \Phi_{i-\frac{1}{2},j}^*}{\Delta x}, \quad *, * = n, n+1, \quad (3.7)$$

and $(f_v)_{ij}^n = \frac{\Psi_{i,j+\frac{1}{2}}^n - \Psi_{i,j-\frac{1}{2}}^n}{\Delta y}$.

Equivalently, the scheme (3.6) can be rewritten as updating $\{\Psi_{i,j-\frac{1}{2}}^n\}_{ij}$ with where

$$\Psi_{i,j-\frac{1}{2}}^{n+1} = \Psi_{i,j-\frac{1}{2}}^n - \frac{\Delta t}{2} \left(\frac{-v_{i,j-2}(f_x)_{i,j-2}^n + 7v_{i,j-1}(f_x)_{i,j-1}^n + 7v_{i,j}(f_x)_{i,j}^n - v_{i,j+1}(f_x)_{i,j+1}^n}{24} \right. \\ \left. + \frac{-v_{i,j-2}(f_x)_{i,j-2}^{n+1} + 7v_{i,j-1}(f_x)_{i,j-1}^{n+1} + 7v_{i,j}(f_x)_{i,j}^{n+1} - v_{i,j+1}(f_x)_{i,j+1}^{n+1}}{24} \right). \quad (3.8)$$

REMARK 4. Such source term evolution by the central difference and a trapezoid rule for time integration has time step restriction and may cause instability if the time step size is too large.

REMARK 5. There is another form of governing equations for f , f_x and f_v in [5, 4],

$$\begin{cases} \frac{\partial f}{\partial t} + v \frac{\partial f}{\partial x} + E(t, x) \frac{\partial f}{\partial v} = 0, \\ \frac{\partial f_x}{\partial t} + v \frac{\partial f_x}{\partial x} + \frac{\partial E(t, x)}{\partial x} f_v + E(t, x) \frac{\partial f_x}{\partial v} = 0, \\ \frac{\partial f_v}{\partial t} + f_x + v \frac{\partial f_v}{\partial x} + E(t, x) \frac{\partial f_v}{\partial v} = 0. \end{cases} \quad (3.9)$$

Then in the context of operator splitting, the third equation in (3.4) will be

$$\frac{\partial f_v}{\partial t} + f_x + v \frac{\partial f_v}{\partial x} = 0. \quad (3.10)$$

We observe that we can only design the SL scheme on $\frac{\partial f_v}{\partial t} + v \frac{\partial f_v}{\partial x} = 0$. It is not mass conservative for f_v with the source term f_x . It lead to the difficulty for writing $(f_v)_{ij}^n$ in a flux difference form as $(f_v)_{ij}^n = \frac{\Psi_{i,j+\frac{1}{2}}^n - \Psi_{i,j-\frac{1}{2}}^n}{\Delta v}$

This SL HWENO scheme may lead to oscillations in large time stepping size when it simulates the VP system mainly from the source term evolution (3.8). We propose to apply the WENO limiter [23, 24] before

HWENO evolution as a pre-processing procedure which is similar to the procedure in [16]. We use the TVB limiter [9, 23, 24] with problem dependent TVB constants to identify troubled cells. For details of the procedure of the limiter, we refer to [24]. Below we provide the flow chart of the conservative SL HWENO with WENO limiters for the VP simulations.

ALGORITHM 1. *Conservative SL HWENO scheme for the VP system.*

Step 1. *Apply WENO limiter as a pre-processing procedure to reconstruct $\Phi_{i+\frac{1}{2},j}^n$.*

First, we use TVB limiter to identify the troubled cells, namely, those cells which might need the limiting procedure. Let:

$$\tilde{f}_{ij} = \Phi_{i+\frac{1}{2},j}^n - f_{ij}^n, \quad \tilde{\tilde{f}}_{ij} = -\Phi_{i-\frac{1}{2},j}^n + f_{ij}^n \quad (3.11)$$

These are modified by the modified minmod function;

$$\tilde{f}_{ij}^{(mod)} = \tilde{m} \left(\tilde{f}_{ij}, f_{i+1,j}^n - f_{ij}^n, f_{ij}^n - f_{i-1,j}^n \right), \quad (3.12)$$

$$\tilde{\tilde{f}}_{ij}^{(mod)} = \tilde{m} \left(\tilde{\tilde{f}}_{ij}, f_{i+1,j}^n - f_{ij}^n, f_{ij}^n - f_{i-1,j}^n \right), \quad (3.13)$$

where \tilde{m} is given by

$$\tilde{m}(a_1, a_2, \dots, a_n) = \begin{cases} a_1 & \text{if } |a_1| \leq M_x(\Delta x)^2, \\ m(a_1, a_2, \dots, a_n) & \text{otherwise,} \end{cases} \quad (3.14)$$

and the minmod function m is given by

$$m(a_1, a_2, \dots, a_n) = \begin{cases} s \cdot \min_{1 \leq j \leq n} |a_j| & \text{if } \text{sign}(a_1) = \text{sign}(a_2) = \dots = \text{sign}(a_n) = s, \\ 0 & \text{otherwise.} \end{cases} \quad (3.15)$$

The TVB limiter parameter $M_x > 0$ is a constant. If $\tilde{f}_{ij}^{(mod)} \neq \tilde{f}_{ij}$ or $\tilde{\tilde{f}}_{ij}^{(mod)} \neq \tilde{\tilde{f}}_{ij}$, we declare the T_{ij} as a troubled cell.

Then we replace $\Phi_{i+\frac{1}{2},j}^n$ and $\Phi_{i-\frac{1}{2},j}^n$ in those troubled cells by WENO reconstruction.

Step 2. *Perform a half time step advection in physical space.*

Step 3. *Compute the electric field at the half step by substituting f^* into equation (3.2) and solve for $E^*(x)$.*

Step 4. *Similar to Step 1, we apply WENO limiter as a pre-processing procedure to reconstruct $\Psi_{i,j+\frac{1}{2}}^*$.*

Step 5. *Perform a full time step advection in velocity space.*

Step 6. *We use the same pre-processing procedure like Step 1 to reconstruct $\Phi_{i+\frac{1}{2},j}^{**}$.*

Step 7. *Perform a half time step advection in physical space.*

4 Numerical tests

In Section 4.1, we first test the performances of the proposed SL HWENO schemes for the 1D transport problem, and then the rigid body rotation was tested by the Strang splitting conservative SL HWENO scheme. In Section 4.2, we demonstrate the utility of the SL HWENO scheme by applying it to classical problems from plasma physics, such as Landau damping and two-stream instability.

4.1 Test problems

EXAMPLE 1. *1D transport problem.*

Consider the linear advection equation:

$$f_t + f_x = 0, \quad x \in [0, 2\pi]. \quad (4.1)$$

The conservative SL methods with fifth order HWENO reconstruction is used to solve equation (4.1). Table 4.1 gives the L_1 error, and the corresponding order of convergence, of both the SL HWENO scheme and the SL WENO scheme when applied to equation (4.1) with smooth initial data

$$f(x, 0) = \sin(x) \quad (0 \leq x \leq 2\pi). \quad (4.2)$$

We observe that these two methods have fifth order accuracy, and the SL HWENO scheme is more accurate than the SL WENO scheme.

Table 4.1: Order of accuracy for (4.1) with $f(x, t = 0) = \sin(x)$ at $T = 20$. $CFL = 1.2$.

N	HWENO		WENO	
	L_1 error	Order	L_1 error	Order
32	4.03E-05	-	7.31E-05	-
64	1.17E-06	5.10	2.23E-06	5.03
96	1.52E-07	5.05	2.93E-07	5.00
128	3.56E-08	5.04	6.97E-08	5.00
160	1.16E-08	5.03	2.28E-08	5.00
192	4.62E-09	5.03	9.16E-09	5.00

Next, to evaluate the capability of the schemes in capturing both discontinuity and smooth solution, we test (4.1) with the initial distribution including four types of profiles

$$f(x, 0) = \begin{cases} \frac{1}{6}(G(x, \beta, z - \delta) + G(x, \beta, z + \delta) + 4G(x, \beta, z)) & \text{for } -0.8 \leq x \leq -0.6, \\ 1 & \text{for } -0.4 \leq x \leq -0.2, \\ 1 - |10(x - 0.1)| & \text{for } 0.0 \leq x \leq 0.2, \\ \frac{1}{6}(F(x, \alpha, a - \delta) + F(x, \alpha, a + \delta) + 4F(x, \alpha, a)) & \text{for } 0.4 \leq x \leq 0.6, \\ 0 & \text{otherwise,} \end{cases} \quad (4.3)$$

where $G(x, \beta, z) = e^{-\beta(x-z)^2}$ and $F(x, \alpha, a) = \sqrt{\max(1 - \alpha^2(x-a)^2, 0)}$. The constants are specified as $a = 0.5, z = -0.7, \delta = 0.005, \alpha = 10$ and $\beta = \frac{\log 2}{36\delta^2}$. The boundary condition is periodic. We compute the solution up to $t = 8$ with 200 points. The results are shown in Figure 4.1. Non-oscillatory numerical capture of discontinuities is observed.

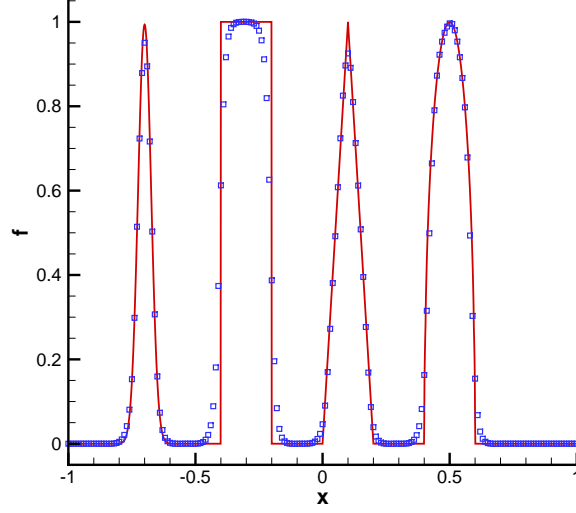


Figure 4.1: The SL HWENO scheme; 200 points, CFL=1.2, T=8.

EXAMPLE 2. *Rigid body rotation.*

Consider the rigid body rotation

$$f_t + v_x(x, y)f_x + v_y(x, y)f_y = 0. \quad (4.4)$$

First, we consider a smooth case for accuracy test. The domain is $[-2\pi, 2\pi] \times [-2\pi, 2\pi]$. The velocity field is given by $v_x(x, y) = -y$, $v_y(x, y) = x$. Table 4.2 gives the error and convergence rates of the scheme for the time step $\Delta t = CFL / (\frac{2\pi}{\Delta x} + \frac{2\pi}{\Delta y})$ with $CFL = 1.2$ for smooth initial data $f(x, y, 0) = \exp(-x^2 - y^2)$. The high order convergence of the scheme is observed.

Table 4.2: Order of accuracy for (4.4) with $f(x, y, t = 0) = \exp(-x^2 - y^2)$ at $T = 2\pi$. $CFL = 1.2$.

N	L_1 error	Order	L_2 error	Order	L_∞ error	Order
20	1.31E-02		2.49E-02		1.19E-01	
40	1.05E-03	3.65	1.90E-03	3.71	1.50E-02	2.99
80	4.34E-05	4.59	8.88E-05	4.42	4.99E-04	4.91
160	2.03E-06	4.42	3.97E-06	4.48	2.11E-05	4.56
320	6.50E-08	4.96	1.36E-07	4.87	7.33E-07	4.85

Secondly, we consider a test case introduced in [20]. The domain is $[-0.5, 0.5]^2$. The velocity field is given by

$$v_x(x, y) = -2\pi y, \quad v_y(x, y) = 2\pi x. \quad (4.5)$$

The initial condition we used is plotted in Figure 4.2. It includes a slotted disk, a cone and a smooth hump. The numerical solutions for the time step $\Delta t = CFL/(\frac{\pi}{\Delta x} + \frac{\pi}{\Delta y})$ with $CFL = 1.2$ after one full revolutions by the conservative SL HWENO scheme (denoted as CSLHWENO-WO) are plotted in Figure 4.2. However, the solution of the scheme without WENO limiter with $CFL = 2.2$ will be oscillatory. We apply the WENO limiter to the scheme (denoted as CSLHWENO-WL). The numerical solution and trouble cells at the last time step are presented in Fig. 4.3. In Fig. 4.4, we plot the 1D cut of the solution compared with the exact solution. Non-oscillatory capturing of discontinuities is observed.

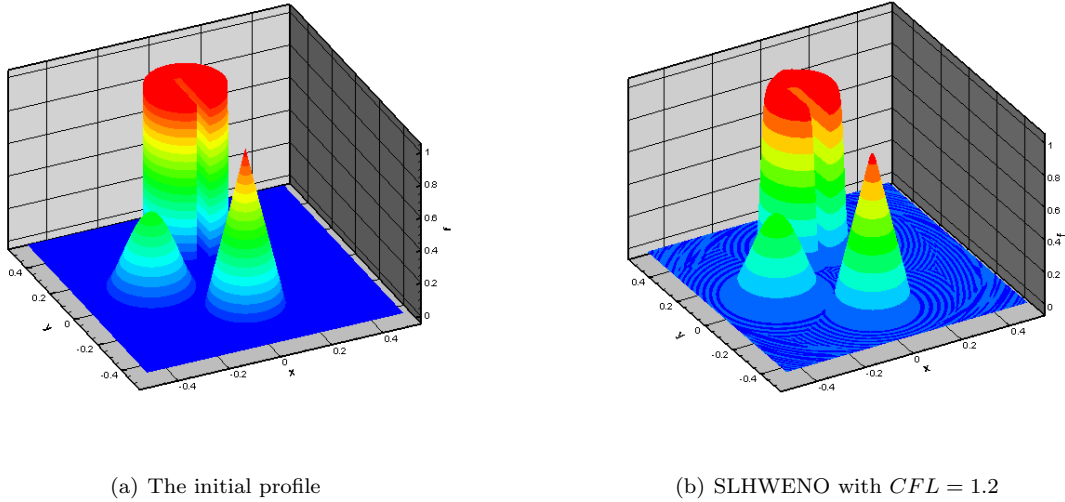


Figure 4.2: Left: Plots of the initial profile. Right: Plots of the numerical solution for equation (4.4) with the velocity field (4.5); $CFL = 1.2$; $T = 1$; The numerical mesh has a resolution of 200×200 ; Conservative SL HWENO scheme without WENO limiter.

4.2 The VP system

In this subsection, we apply the conservative SL HWENO scheme to the VP system. Periodic boundary conditions are imposed in the x -direction and zero boundary conditions are imposed in the v -direction for all of our test problems. Because of the periodicity in space, a fast Fourier transform (FFT) is used to solve the 1-D Poisson equation. $\rho(x, t)$ is computed by the rectangular rule, $\rho(x, t) = \int f(x, v, t) dv = \sum_j f(x, v_j, t) \Delta v$, which is spectrally accurate [6], when the underlying function is smooth enough. We recall several norms in the VP

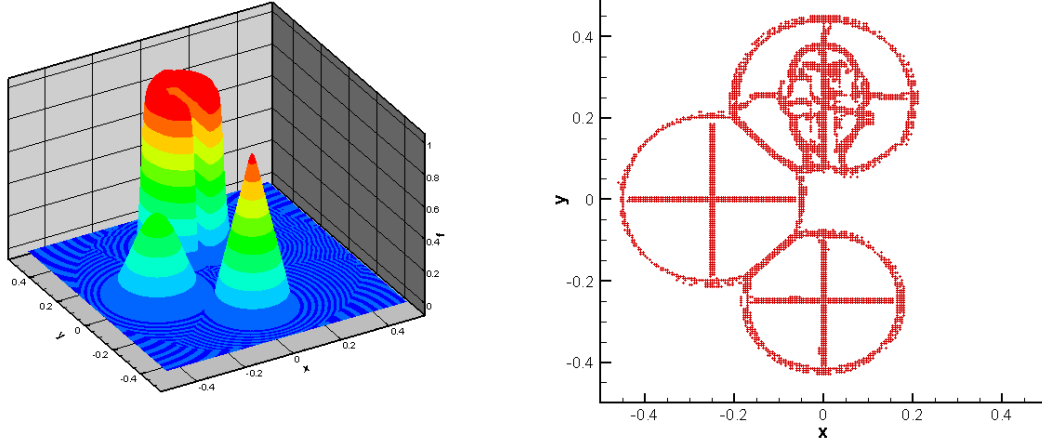


Figure 4.3: Left: The numerical solution for equation (4.4) with the velocity field (4.5). Right: Trouble cells. $CFL = 2.2$. TVB constant $M = 1.0$. $T = 1$. The numerical mesh has a resolution of 200×200 . Conservative SL HWENO scheme with WENO limiter.

system below, which remain constant in time.

1. L^p norm $1 \leq p \leq \infty$:

$$\|f\|_p = \left(\int_v \int_x |f(x, v, t)|^p dx dv \right)^{\frac{1}{p}} \quad (4.6)$$

2. Energy:

$$Energy = \int_v \int_x f(x, v, t) v^2 dx dv + \int_x E^2(x, t) dx, \quad (4.7)$$

where $E(x, t)$ is the electric field.

3. Entropy:

$$Entropy = \int_v \int_x f(x, v, t) \log(f(x, v, t)) dx dv. \quad (4.8)$$

Tracking relative deviations of these quantities numerically will be a good measurement of the quality of numerical schemes. The relative deviation is defined to be the deviation away from the corresponding initial value divided by the magnitude of the initial value. It is expected that our scheme will conserve mass. However, the positivity of f will not be preserved. Thus, when numerically computing the entropy, we compute $\int_v \int_x f(x, v, t) \log |f(x, v, t)| dx dv$. We set the time step by $\Delta t = CFL / (v_{max}/\Delta x + \max(E(x))/\Delta y)$, where v_{max} is the maximum velocity on the phase space mesh.

In the following, we test the conservative SL HWENO scheme with $CFL = 1.2$, denoted as "CSLHWENO-WO", to solve the VP system. This schemes will be compared with the fifth order conservative SL WENO

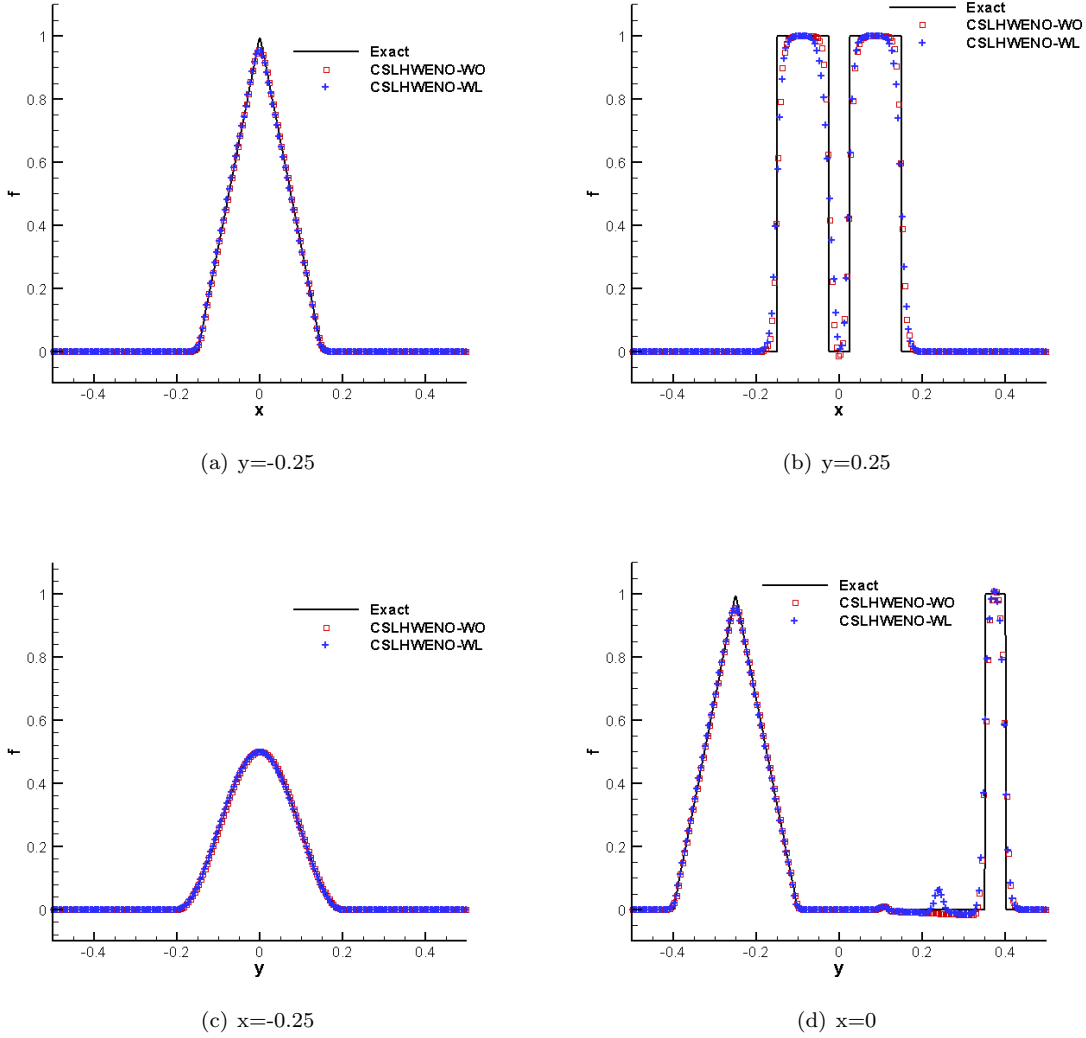


Figure 4.4: Plots of the 1D cuts of the numerical solution for equation (4.4) at $y = -0.25, y = 0.25, x = -0.25, x = 0$ (from top left to bottom right). The solid line depicts the exact solution. The numerical mesh has a resolution of 200×200 .

scheme proposed in [26] with the same $CFL = 1.2$, denoted as "CSLWENO". Moreover, we will study the conservative SL HWENO scheme with the large $CFL = 2.2$. In this case, the WENO limiter in certain TVB constants is needed to enforce the stability of this scheme, and denote the scheme as "CSLHWENO-WL".

EXAMPLE 3. *Weak Landau damping.*

Consider the weak Landau damping for the VP system. The initial condition used here is,

$$f(x, v, t = 0) = \frac{1}{\sqrt{2\pi}} (1 + \alpha \cos(kx)) \exp\left(-\frac{v^2}{2}\right), \quad (4.9)$$

with $\alpha = 0.01$ and $k = 0.5$. Our simulation parameters are $v_{max} = 5$, $N_x = 64$, $N_v = 128$. The time evolution of the L^2 and L^∞ norms of the electric field (in semi-log scale) are plotted in the upper plots of Figure 4.5. The

correct damping of the electric field of CSLWENO and CSLHWENO-WO is observed in the plots, benchmarked with the theoretical value $\gamma = 0.1533$ [14] (the solid line in the same plots). We observe that the conservative SL scheme generates very consistent results, performing very well in recovering the damping rate. Time evolution of the relative deviations of the L^1 , L^2 solution norms, energy, entropy in the discrete sense are demonstrated in the middle and bottom plots in Figure 4.5. The advantage of using conservative schemes in preserving the relevant physical norms is observed. CSLHWENO-WO is observed to perform slightly better than the CSLWENO in preserving norms.

EXAMPLE 4. *Strong Landau damping.*

Consider the strong Landau damping for the VP system. We simulate the VP system with the initial condition in equation (4.9) with $\alpha = 0.5$ and $k = 0.5$. Our simulation parameters are $v_{max} = 5$, $N_x = 128$, $N_v = 256$. In the first row of Figure 4.6, the time evolution of the L^2 and L^∞ norms of the electric field with the linear decay rate $\gamma_1 = -0.2812$ and $\gamma_2 = 0.0770$ [7, 16] (in semi-log scale) are plotted. The Time evolution of the relative deviations of discrete L^1 norm, L^2 norm, kinetic energy and entropy for CSLWENO and CSLHWENO-WO are plotted in the second and third rows of Figure 4.6. CSLHWENO-WO scheme is observed to perform slightly better in preserving these norms than the CSLWENO scheme. In Figure 4.7, numerical solutions of CSLWENO and CSLHWENO-WO at $t = 30$ are plotted. Compared with CSLWENO, slightly better resolution is observed for CSLHWENO-WO. The results of conservative SL scheme with $CFL = 2.2$ by WENO limiter as well as the trouble cells in the last step of the CSLHWENO-WL evolution are presented in the bottom plots of Figure 4.7. The results of CSLHWENO-WL ($CFL = 2.2$) are observed to be comparable to those of CSLHWENO-WO ($CFL = 1.2$). It is also observed that when the filamentation structures become under-resolved by the numerical mesh, trouble cells are identified and WENO limiters are applied.

EXAMPLE 5. *Two stream instability [13].*

Consider two stream instability, with an unstable initial distribution function,

$$f(x, v, t = 0) = \frac{2}{7\sqrt{2\pi}}(1 + 5v^2)(1 + \alpha((\cos(2kx) + \cos(3kx))/1.2 + \cos(kx))) \exp\left(-\frac{v^2}{2}\right)$$

with $\alpha = 0.01$, $k = 0.5$. The length of the domain in the x direction is $L = \frac{2\pi}{k}$ and the background ion distribution function is fixed, uniform and chosen so that the total net charge density for the system is zero. Our numerical simulation parameters are $v_{max} = 5$, $N_x = 64$, $N_v = 128$. In the first row of Figure 4.8, the time

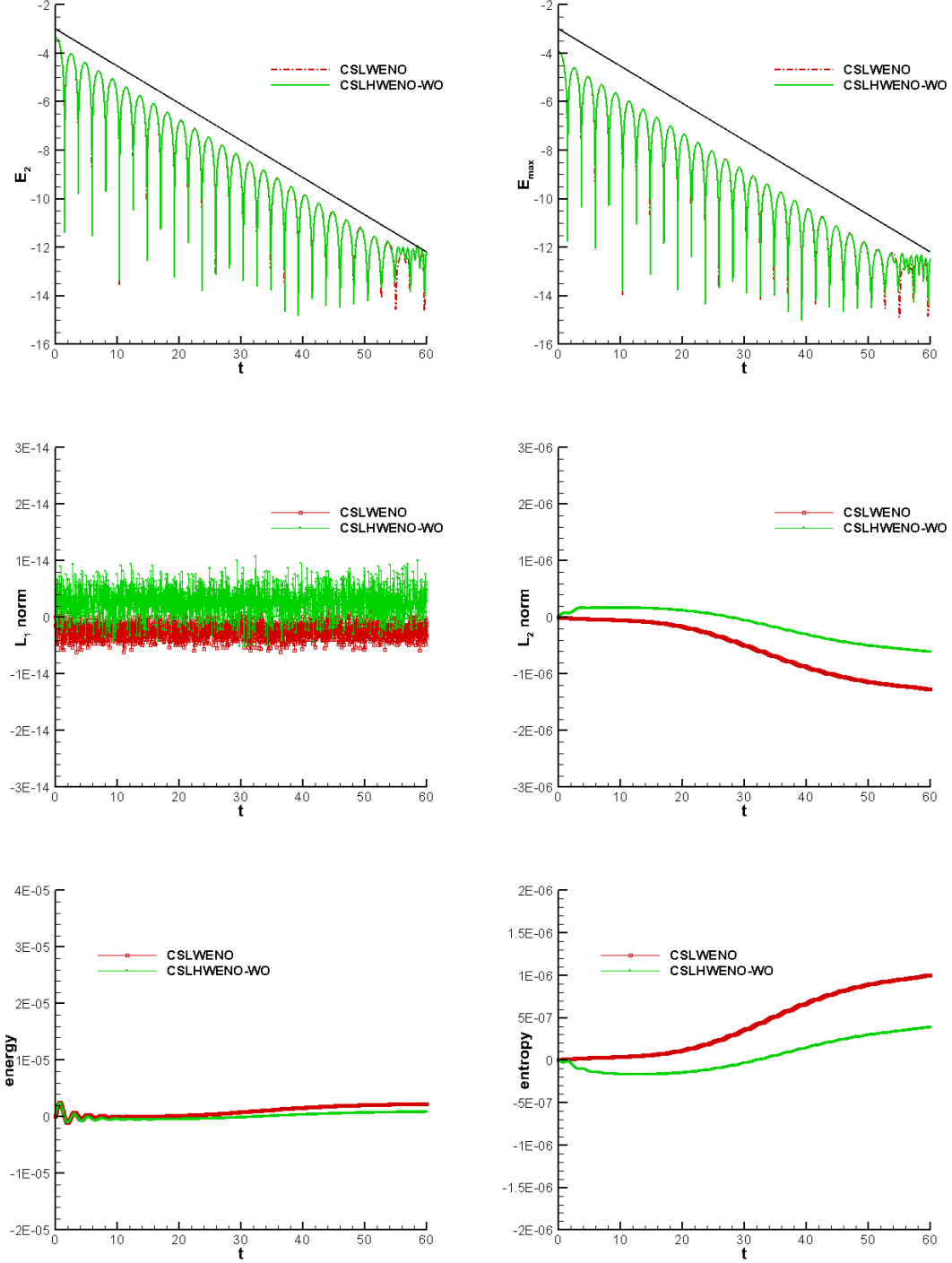


Figure 4.5: Weak Landau damping: time evolution of the electric field in L^2 (upper left) and L^∞ (upper right) norms, Time evolution of the relative deviations of L^1 (middle left) and L^2 (middle right) norms of the solution as well as the discrete kinetic energy (lower left) and entropy (lower right).

evolution of the L^2 and L^∞ norms of the electric field (in semi-log scale) for CSLWENO and CSLHWENO-WO are presented. Comparable results of the discrete L^1 norm, L^2 norm, kinetic energy and entropy for CSLWENO

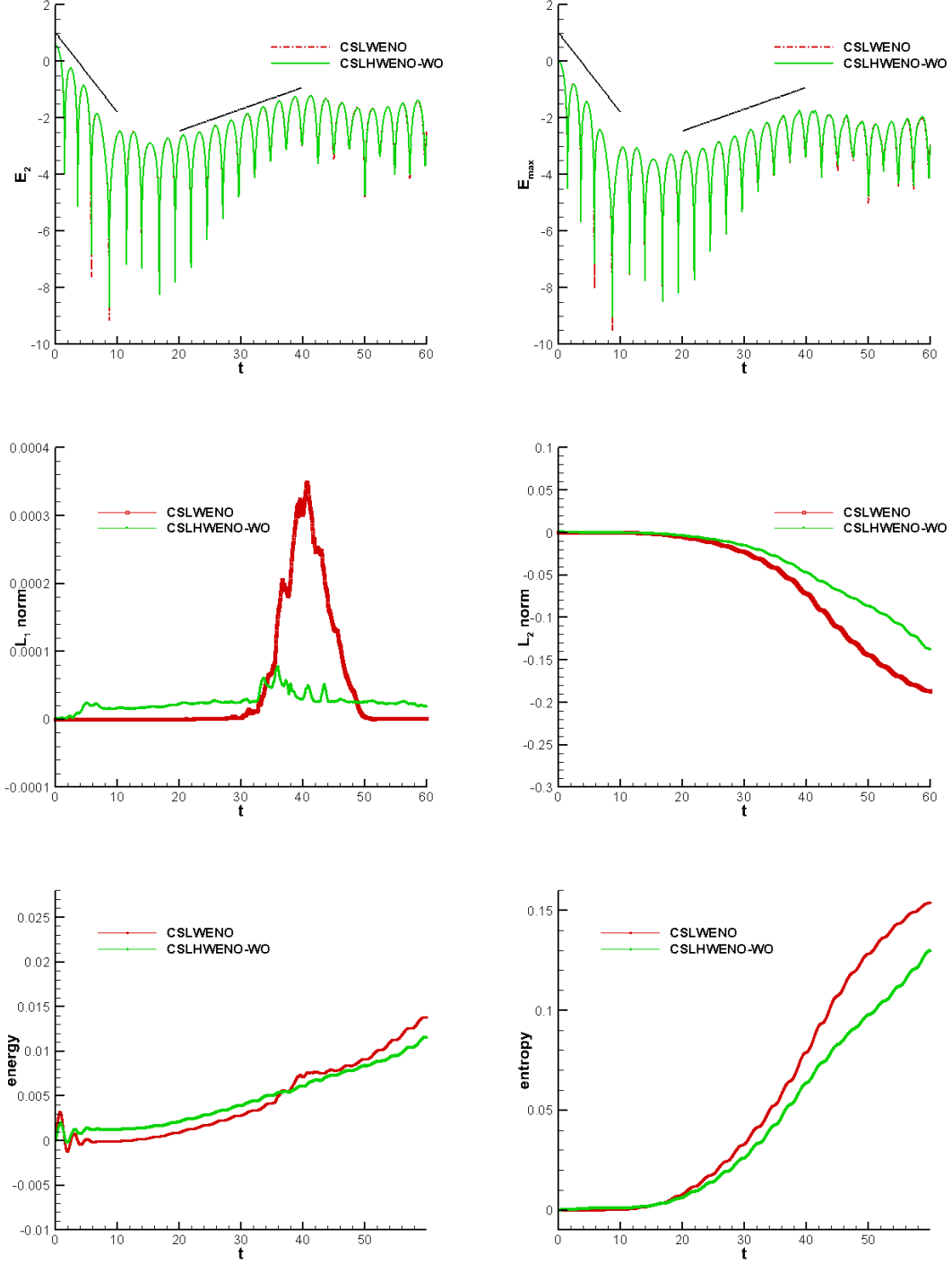


Figure 4.6: Strong Landau damping: time evolution of the electric field in L^2 (upper left) and L^∞ (upper right) norms, time evolution of the relative deviations of L^1 (middle left) and L^2 (middle right) norms of the solution as well as the discrete kinetic energy (lower left) and entropy (lower right).

and *CSLHWENO-WO* are observed in the second and third rows of Figure 4.8. In Figure 4.9, we show numerical solutions at $T = 53$ of *CSLWENO*, *CSLHWENO-WO* and *CSLHWENO-WL*. Comparable solutions are observed

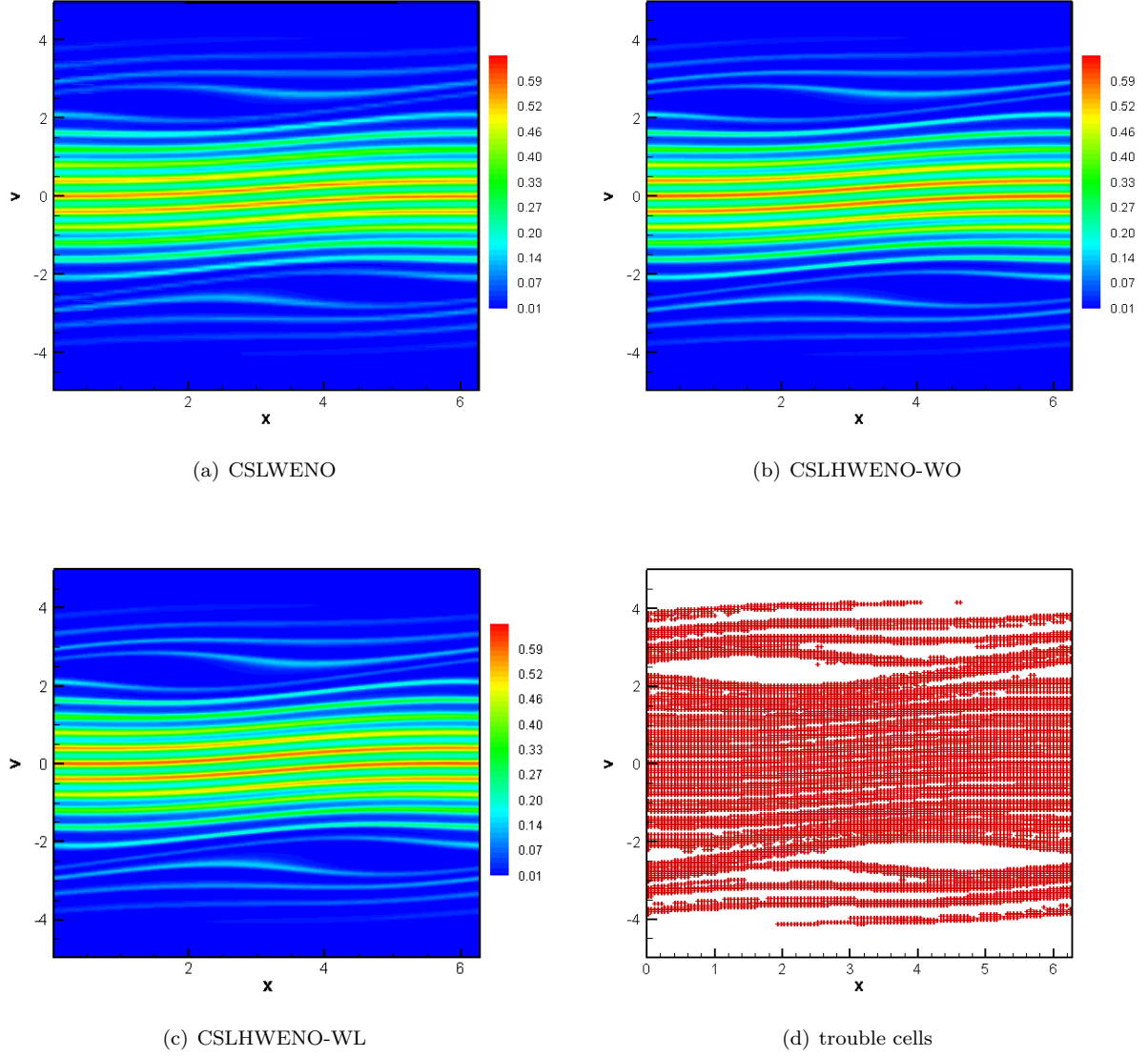


Figure 4.7: Strong Landau damping. $T = 30$. $N_x \times N_v = 128 \times 256$. Top left: CSLWENO. Top right: CSLHWENO-WO ($CFL = 1.2$). Bottom left: CSLHWENO-WL ($CFL = 2.2$); the TVB constants $M_x = M_y = 1$. Bottom right: trouble cells of CSLHWENO-WL at the last time step.

for the CSLWENO ($CFL = 1.2$), CSLHWENO-WO ($CFL = 1.2$) and CSLHWENO-WL ($CFL = 2.2$). Note that the solution of CSLHWENO-WO at $CFL = 2.2$ (not presented here) will be oscillatory without the limiter.

EXAMPLE 6. *Two stream instability* [32, 10].

Consider the symmetric two stream instability,

$$f(x, v, t = 0) = \frac{1}{2v_{th}\sqrt{2\pi}} \left[\exp\left(-\frac{(v-u)^2}{2v_{th}^2}\right) + \exp\left(-\frac{(v+u)^2}{2v_{th}^2}\right) \right] (1 + 0.05 \cos(kx))$$

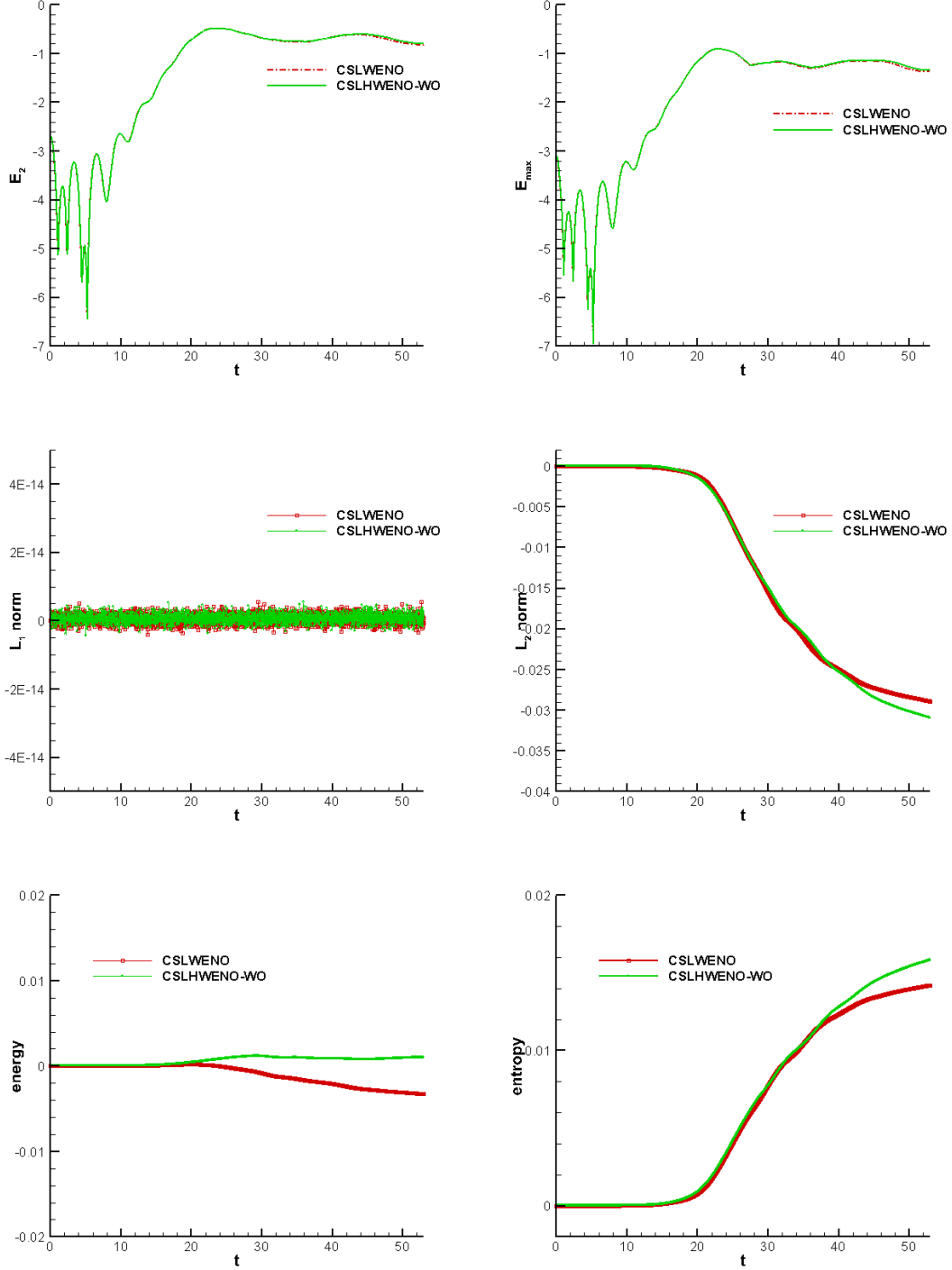


Figure 4.8: Two-stream instability: time evolution of the electric field in L^2 (upper left) and L^∞ (upper right) norms, time evolution of the relative deviations of L^1 (middle left) and L^2 (middle right) norms of the solution as well as the discrete kinetic energy (lower left) and entropy (lower right) for CSLWENO and CSLHWENO-WO.

with $u = 0.99$, $v_{th} = 0.3$ and $k = \frac{2}{13}$. Our numerical simulation parameters are $v_{max} = 5$, $N_x = 512$, $N_v = 512$.

In the first row of Figure 4.10, the time evolution of the L^2 and L^∞ norms of the electric field (in semi-log scale)

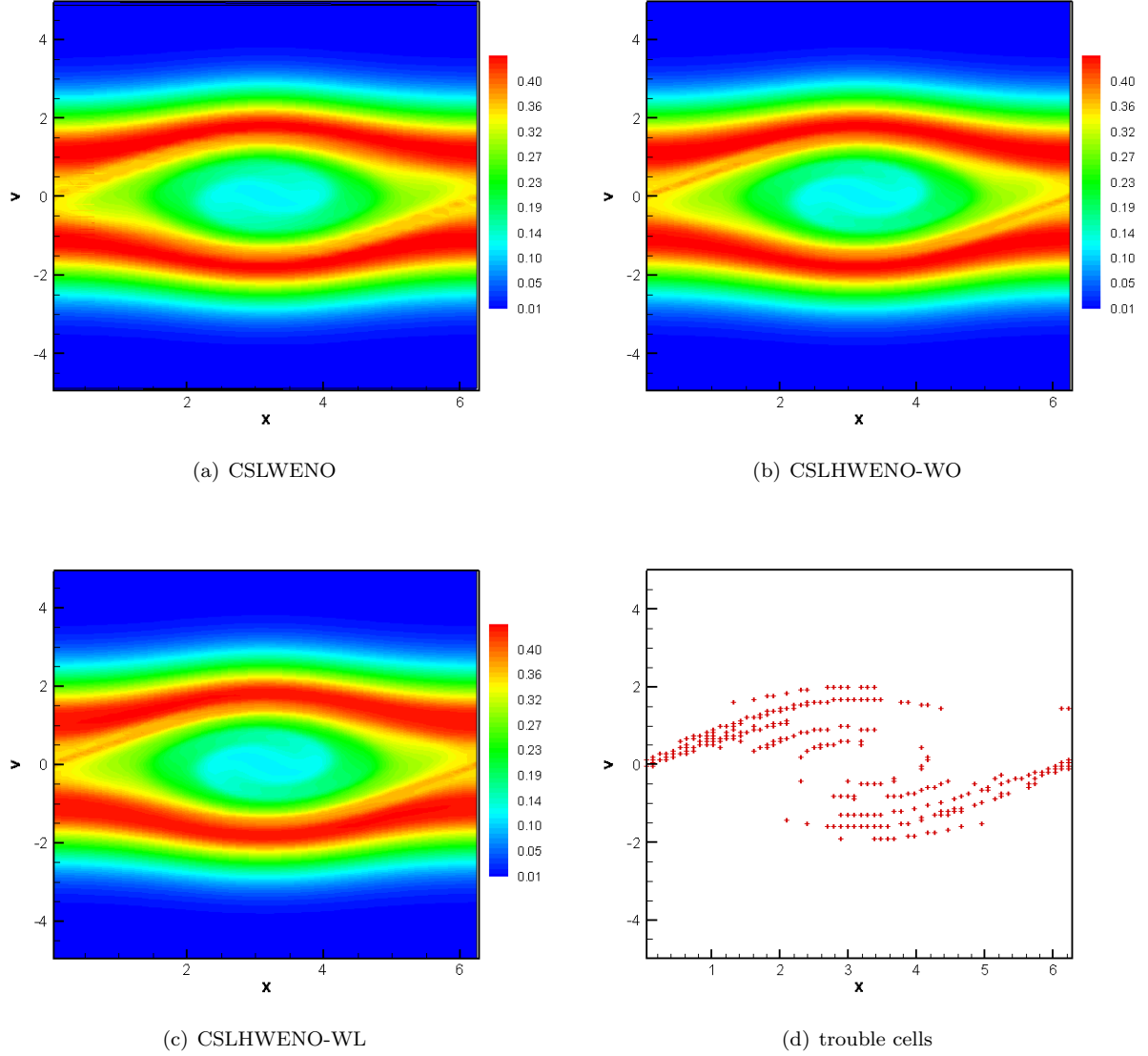


Figure 4.9: Phase space plots of the two stream instability at $T = 53$. The numerical mesh is 64×128 . Top left: CSLWENO. Top right: CSLHWENO-WO ($CFL = 1.2$). Bottom left: CSLHWENO-WL ($CFL = 2.2$); the TVB constants $M_x = 1, M_y = 10$. Bottom right: trouble cells of CSLHWENO-WL at the last time step.

for CSLWENO and CSLHWENO-WO are plotted. Figure 4.11 shows numerical solutions of phase space profiles for CSLWENO, CSLHWENO-WO and CSLHWENO-WL at $T = 70$. The TVB constants of CSLHWENO-WL are $M_x = M_y = 0.1$.

5 Conclusions

In this paper, we propose a conservative SL HWENO scheme for VP system based on dimensional splitting. Compared with the original WENO reconstruction, the advantage of HWENO reconstruction is compact. To

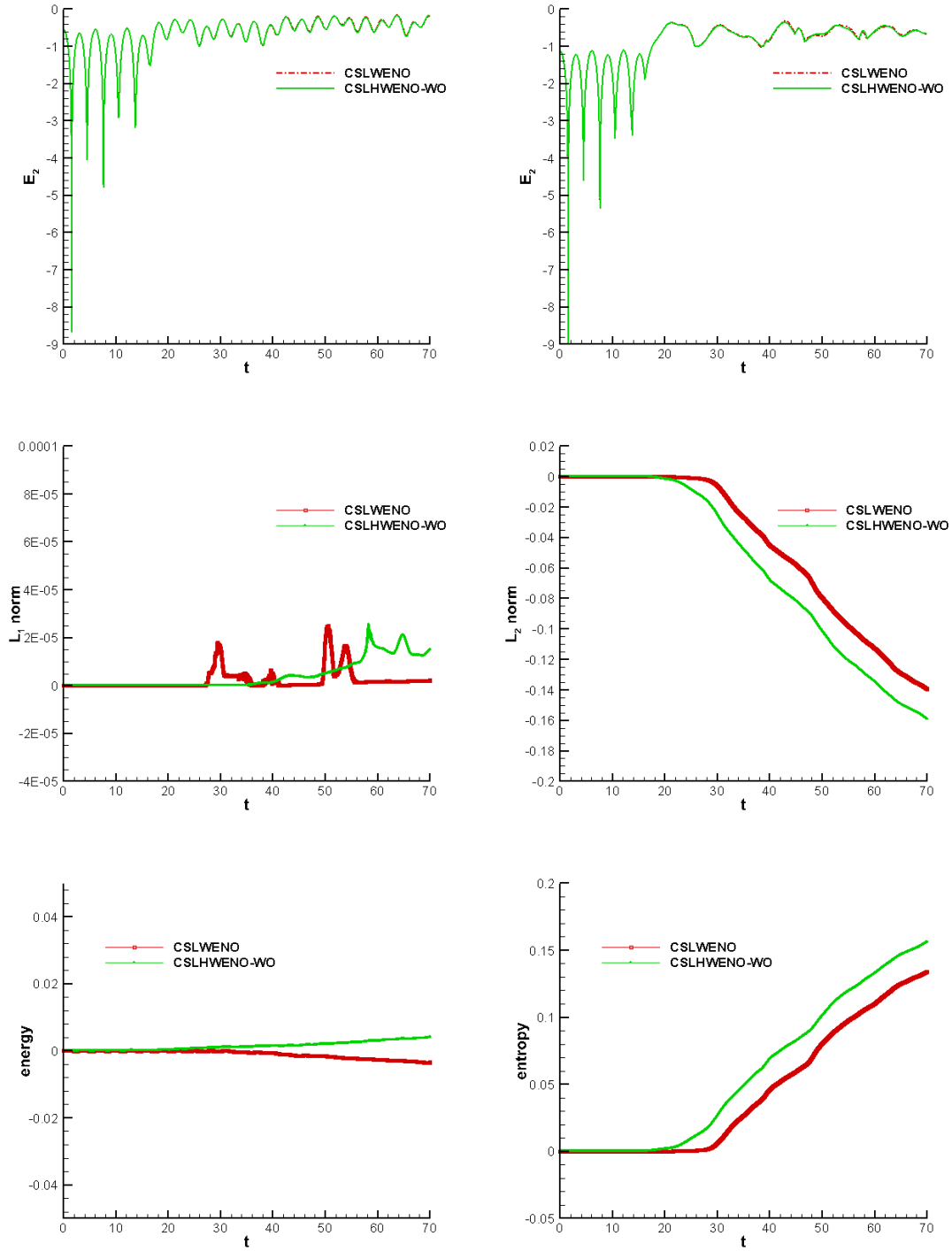


Figure 4.10: Two-stream instability: time evolution of the electric field in L^2 (upper left) and L^∞ (upper right) norms, L^1 (middle left) and L^2 (middle right) norms of the solution as well as the discrete kinetic energy (lower left) and entropy (lower right).

ensure local mass conservation, the derivative in the scheme is rewritten as the flux-difference form. The fifth order conservative SL HWENO scheme for the flux difference is proposed. The scheme can be extended to solve

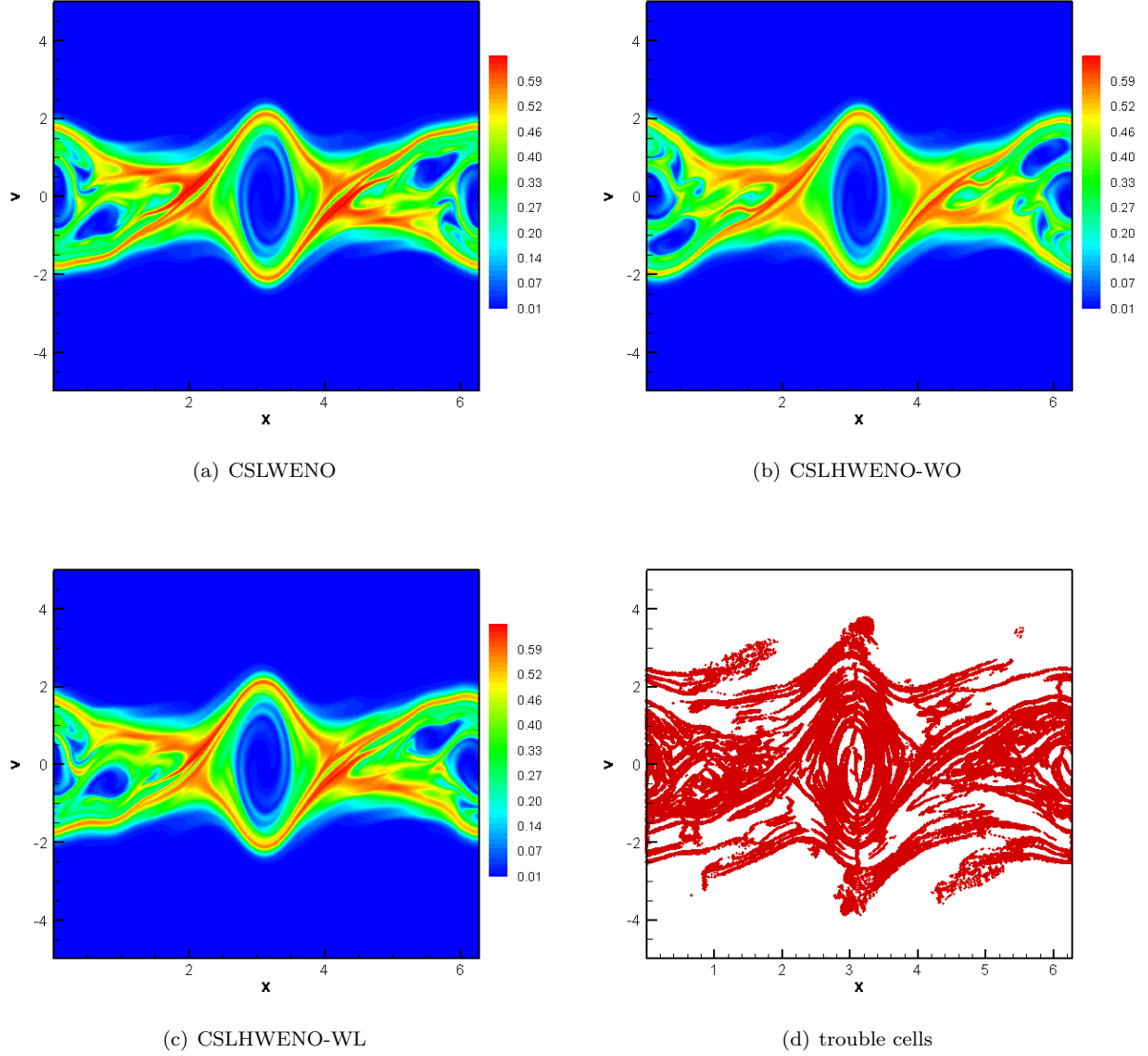


Figure 4.11: Phase space plots of the two stream instability at $T = 70$. The numerical mesh is 512×512 . Top left: CSLWENO. Top right: CSLHWENO-WO ($CFL = 1.2$). Bottom left: CSLHWENO-WL ($CFL = 2.2$). Bottom right: trouble cells of CSLHWENO-WL at the last time step.

high dimensional problem by the Strang splitting method. We show the SL HWENO scheme with the Eulerian CFL condition perform well for the classical Landau damping and the two-stream instability in plasma physics. When the time stepping size is larger than the Eulerian CFL restriction, we introduce WENO limiters to control oscillations.

References

- [1] B. AYUSO, J. A. CARRILLO, AND C.-W. SHU, *Discontinuous Galerkin methods for the one-dimensional*

- Vlasov-Poisson system*, Kinetic and Related Models, 4 (2011), pp. 955–989.
- [2] D. BARNES, T. KAMIMURA, J.-N. LEBOEUF, AND T. TAJIMA, *Implicit particle simulation of magnetized plasmas*, Journal of Computational Physics, 52 (1983), pp. 480–502.
 - [3] J. BARNES AND P. HUT, *A hierarchical $O(N \log N)$ force-calculation algorithm*, Nature, (1986).
 - [4] N. BESSE, *Convergence of a high-order semi-Lagrangian scheme with propagation of gradients for the one-dimensional Vlasov-Poisson system*, SIAM Journal on Numerical Analysis, 46 (2008), pp. 639–670.
 - [5] N. BESSE AND E. SONNENDRÜCKER, *Semi-Lagrangian schemes for the Vlasov equation on an unstructured mesh of phase space*, Journal of Computational Physics, 191 (2003), pp. 341–376.
 - [6] J. P. BOYD, *Chebyshev and Fourier spectral methods*, Courier Corporation, 2001.
 - [7] C.-Z. CHENG AND G. KNORR, *The integration of the Vlasov equation in configuration space*, Journal of Computational Physics, 22 (1976), pp. 330–351.
 - [8] Y. CHENG, I. M. GAMBA, AND P. J. MORRISON, *Study of conservation and recurrence of Runge-Kutta discontinuous Galerkin schemes for Vlasov-Poisson systems*, Journal of Scientific Computing, 56 (2013), pp. 319–349.
 - [9] B. COCKBURN AND C.-W. SHU, *Runge-Kutta discontinuous Galerkin methods for convection-dominated problems*, Journal of Scientific Computing, 16 (2001), pp. 173–261.
 - [10] N. CROUSEILLES, M. MEHRENBARGER, AND E. SONNENDRÜCKER, *Conservative semi-Lagrangian schemes for Vlasov equations*, Journal of Computational Physics, 229 (2010), pp. 1927–1953.
 - [11] B. A. DE DIOS, J. A. CARRILLO, AND C.-W. SHU, *Discontinuous Galerkin methods for the multi-dimensional Vlasov-Poisson problem*, Mathematical Models and Methods in Applied Sciences, 22 (2012), p. 1250042.
 - [12] E. EVSTATIEV AND B. SHADWICK, *Variational formulation of particle algorithms for kinetic plasma simulations*, Journal of Computational Physics, 245 (2013), pp. 376–398.
 - [13] F. FILBET AND E. SONNENDRÜCKER, *Comparison of eulerian vlasov solvers*, Computer Physics Communications, 150 (2003), pp. 247–266.

- [14] F. FILBET, E. SONNENDRÜCKER, AND P. BERTRAND, *Conservative numerical schemes for the Vlasov equation*, Journal of Computational Physics, 172 (2001), pp. 166–187.
- [15] A. FRIEDMAN, S. PARKER, S. RAY, AND C. BIRDSALL, *Multi-scale particle-in-cell plasma simulation*, Journal of Computational Physics, 96 (1991), pp. 54–70.
- [16] W. GUO AND J.-M. QIU, *Hybrid semi-Lagrangian finite element-finite difference methods for the Vlasov equation*, Journal of Computational Physics, 234 (2013), pp. 108–132.
- [17] R. HEATH, I. M. GAMBA, P. J. MORRISON, AND C. MICHLER, *A discontinuous Galerkin method for the Vlasov–Poisson system*, Journal of Computational Physics, 231 (2012), pp. 1140–1174.
- [18] G. JACOBS AND J. S. HESTHAVEN, *High-order nodal discontinuous Galerkin particle-in-cell method on unstructured grids*, Journal of Computational Physics, 214 (2006), pp. 96–121.
- [19] G.-S. JIANG AND C.-W. SHU, *Efficient Implementation of Weighted ENO Schemes*, Journal of Computational Physics, 126 (1996), pp. 202–228.
- [20] R. LEVEQUE, *High-resolution conservative algorithms for advection in incompressible flow*, SIAM Journal on Numerical Analysis, (1996), pp. 627–665.
- [21] H. LIU AND J. QIU, *Finite difference Hermite WENO schemes for hyperbolic conservation laws*, Journal of Scientific Computing, 63, pp. 548–572.
- [22] T. NAKAMURA AND T. YABE, *Cubic interpolated propagation scheme for solving the hyper-dimensional VlasovPoisson equation in phase space*, Computer Physics Communications, 120 (1999), pp. 122–154.
- [23] J. QIU AND C.-W. SHU, *Hermite WENO schemes and their application as limiters for Runge–Kutta discontinuous Galerkin method: one-dimensional case*, Journal of Computational Physics, 193 (2004), pp. 115–135.
- [24] ———, *Runge–Kutta discontinuous Galerkin method using WENO limiters*, SIAM Journal on Scientific Computing, 26 (2005), pp. 907–929.
- [25] J.-M. QIU AND A. CHRISTLIEB, *A conservative high order semi-Lagrangian WENO method for the Vlasov equation*, Journal of Computational Physics, 229 (2010), pp. 1130–1149.

- [26] J.-M. QIU AND C.-W. SHU, *Conservative high order semi-Lagrangian finite difference WENO methods for advection in incompressible flow*, Journal of Computational Physics, 230 (2011), pp. 863–889.
- [27] ———, *Conservative semi-Lagrangian finite difference WENO formulations with applications to the Vlasov equation*, Communications in Computational Physics, 10 (2011), pp. 979–1000.
- [28] J.-M. QIU AND C.-W. SHU, *Positivity preserving semi-Lagrangian discontinuous Galerkin formulation: theoretical analysis and application to the Vlasov-Poisson system*, Journal of Computational Physics, 230 (2011), pp. 8386–8409.
- [29] J. A. ROSSMANITH AND D. C. SEAL, *A positivity-preserving high-order semi-Lagrangian discontinuous Galerkin scheme for the Vlasov-Poisson equations*, Journal of Computational Physics, 230 (2011), pp. 6203–6232.
- [30] C.-W. SHU AND S. OSHER, *Efficient implementation of essentially non-oscillatory shock-capturing schemes, II*, Journal of Computational Physics, 83 (1989), pp. 32–78.
- [31] E. SONNENDRÜCKER, J. ROCHE, P. BERTRAND, AND A. GHIZZO, *The semi-Lagrangian method for the numerical resolution of the Vlasov equation*, Journal of computational physics, 149 (1999), pp. 201–220.
- [32] T. UMEDA, *A conservative and non-oscillatory scheme for Vlasov code simulations*, Earth, planets and space, 60 (2008), pp. 773–779.
- [33] T. XIONG, J.-M. QIU, Z. XU, AND A. CHRISTLIEB, *High order maximum principle preserving semi-Lagrangian finite difference WENO schemes for the Vlasov equation*, Journal of Computational Physics, 273 (2014), pp. 618–639.
- [34] T. YABE, F. XIAO, AND T. UTSUMI, *The constrained interpolation profile method for multiphase analysis*, Journal of Computational physics, 169 (2001), pp. 556–593.
- [35] C. YANG AND F. FILBET, *Conservative and non-conservative methods based on Hermite weighted essentially non-oscillatory reconstruction for Vlasov equations*, Journal of Computational Physics, 279 (2014), pp. 18–36.
- [36] S. ZAKI, T. BOYD, AND L. GARDNER, *A finite element code for the simulation of one-dimensional Vlasov plasmas. II. Applications*, Journal of Computational Physics, 79 (1988), pp. 200–208.

- [37] S. ZAKI, L. GARDNER, AND T. BOYD, *A finite element code for the simulation of one-dimensional Vlasov plasmas. I. Theory*, Journal of Computational Physics, 79 (1988), pp. 184–199.
- [38] T. ZHOU, Y. GUO, AND C.-W. SHU, *Numerical study on Landau damping*, Physica D: Nonlinear Phenomena, 157 (2001), pp. 322–333.
- [39] J. ZHU AND J. QIU, *A class of the fourth order finite volume Hermite weighted essentially non-oscillatory schemes*, Science in China Series A: Mathematics, 51 (2008), pp. 1549–1560.